AN ABSTRACT OF THE THESIS OF

Vincent C. Korthuis for the degree of Doctor of Philosophy in chemistry, presented on November 1, 1994.

Title: New Oxides of Vanadium with Unusual Properties

Abstract approved: Redacted for Privacy

Dr. A.W. Sleight

This was an exploratory synthesis program aimed at preparing new oxides of vanadium which might have interesting and/or useful properties. No particular structures or properties were sought.

Unique thermal expansion properties were discovered for new $(Zr,Hf)(V,P)_2O_7$ compositions. Some of these compositions showed negative thermal expansion over a wide temperature range up to at least 900 °C. An understanding of this unusual behavior was sought using differential scanning calorimetry, thermal gravimetric analysis, X-ray diffraction, neutron diffraction, NMR and modeling.

Compounds of the type A_2VPO_6 (A = Li, Na or K) were prepared for the first time. All have structural features not previously observed. The Na and K compounds are isostructural and contain helical chains formed from phosphate tetrahedra and vanadate square pyramids. The

$(VPO_6)^{2-}$ chains are held together by Na^+ or K^+ cations. In the Li_2VPO_6 structure, $(VPO_6)^{2-}$ sheets are held together by Li^+ cations. Although many layered phosphates are known, this is a new type of sheet which is formed from phosphate tetrahedra and vanadate octahedra. The ionic conductivities for the A_2VPO_6 compounds were determined and found to be low.

New compounds were also found in the A/V/Bi/O (A = Li, Na, K), Al/V/Bi/O and K/Pb/P/O systems. Characterization of these compounds was attempted and led to known structure types or structures could not be solved.

New Oxides of Vanadium with Unusual Properties

by

Vincent Korthuis

A THESIS

Submitted to

OREGON STATE UNIVERSITY

in partial fulfillment of

the requirements for the

degree of

Doctor of Philosophy

Completed November 1, 1994
Commencement June 1995

Doctor of Philosophy thesis of Vincent C. Korthuis
presented on November 1, 1994

APPROVED:

Redacted for Privacy

Professor of Chemistry in charge of major

Redacted for Privacy

Head of Department of Chemistry

Redacted for Privacy

Dean of Graduate School

I understand that my thesis will become part of the permanent collection of Oregon State University libraries. My Signature below authorizes release of my thesis to any reader upon request.

Redacted for Privacy

Vincent C. Korthuis

ACKNOWLEDGEMENTS

I would like to thank Dr. Sleight for his direction and instruction as well as support throughout my research. I am honored to have been instructed by such a distinguished scientist.

I would also like to thank the members of Dr. Sleight's group. I thank Dr. Jinfan Huang for helping me get started with my research, Dr. Rolf-Dieter Hoffman for teaching me the basics of crystallography, as well as his friendly personality and time to help me with my research goals. I thank Phong Nguyen for helping me learn new concepts as well as being a good friend. I thank Dr. Ruiping Wang and Dr. Laura King for their expertise in the field of physics. I thank Ammar Kamadoli, Sasirekha (Sasi) Kodialam, Pat Woodward, Nazy Khosrovn, Paul Bacon, and Matt Hall for their discussions as well as their friendship.

I want to thank my parents, Larry and Sarah King and Les and Lorna Molenaar for their endless support. A special thank you goes to my wife Debbie who has waited patiently and encouraged me to work hard to obtain my goals.

TABLE OF CONTENTS

TABLE OF CONTENTS (CONTINUED)

LIST OF FIGURES

LIST OF FIGURES (CONTINUED)

LIST OF TABLES

LIST OF TABLES (CONTINUED)

New Oxides of Vanadium with Unusual Properties

1. INTRODUCTION

1.1 Introduction of research

My research has focused on discovering new oxides containing vanadium, hafnium and/or zirconium. One motivation was to obtain new compounds and thereby broaden our knowledge of materials, properties, and the boundaries of the solid state by a purely exploratory approach to synthesis. The other approach in my research was to prepare new materials by design for a subsequent study of physical properties. Then from the knowledge of the physical properties, we would attempt to design and develop materials with enhanced properties for new novel inorganic materials applications.

Exploratory synthesis aimed at obtaining new materials using solid state reactions frequently yields already known phases and inhomogoneous products. Although time consuming, this high risk research may be very rewarding if one obtains new materials that have properties which are interesting for scientific or technology reasons. Exploratory research on vanadium containing compounds is described in Chapter 2.

The investigation of vanadium containing systems led to the synthesis of three new compounds with the general formula A_2VPO_6 (A=Li, Na, and K). Two new compounds Na_2VPO_6 and K_2VPO_6 are isostructural, but a different structure is found for Li_2VPO_6. Difficulty working with this system is the glass forming tendency of both vanadium and phosphorous oxides (1,2). The synthesis and the structure determination of both Na_2VPO_6 and K_2VPO_6 will be discussed in Chapter 3.

The synthesis and structure of Li_2VPO_6 is quite different than that of the above two compounds. This compound melts incongruently and crystallizes in an acentric space group which is capable of producing a second harmonic signal. Investigation and discussion, of this system are presented in Chapter 4.

After the A_2VPO_6 compounds were synthesized and the crystal structure solved, observation of the large isotropic B values of the alkali metals led to the investigation of the possibility of ionic conduction. The search for highly conductive ionic materials has become a very specialized field. With the environment as one of the publics concern, solid state materials may some day replace the conventional lead acid battery as well as the alkali battery. Some of the advantages of solid state batteries are that they will weigh less, and the volume occupied by the reactants is lower for the power output

obtainable. Some of the disadvantages are the normally high temperatures required to maintain the high conduction as well as finding an ionic conductor that is inert to the reactants at these temperatures. The investigation of ionic conductivity of the A_2VPO_6 (A= K, Na and Li) compounds is discussed in Chapter 5.

Exploratory investigation into the zirconium oxide and vanadium oxide system led to the formation of small crystals of ZrV_2O_7, a compound which was first discovered by Peyronel (3). This compound was found to have an interesting negative thermal expansion behavior by Craig and Hummel (4). According to Hummel's classification of low expansion materials(5), only those that have a thermal expansion coefficient(α) less than 2.0×10^{-6} $^{\circ}C^{-1}$ are considered low thermal expansion materials. Only three low expansion oxide materials were known before World War II, fused silica glass ($\alpha = 0.50 \times 10\text{-}6$ $^{\circ}C^{-1}$)(6), vycor glass ($\alpha = 0.80 \times 10^{-6}$ $^{\circ}C^{-1}$) (6), and cordierite($\alpha = 1.40 \times 10^{-6}$ $^{\circ}C^{-1}$)(7,8). Since then, much research has been done to develop other low thermal expansion materials and to analyze their behavior based on phase relations, stability, crystallization, and crystal chemistry. Many new materials having low thermal expansion behavior over different temperature ranges have now been reported (9,10,11,12,13,14).

Many potential applications for low expansion materials have been studied. The auto industry is very interested in new light weight thermally stable low expansion materials for use in many engine parts such as exhaust port liners and insulation for the exhaust manifold to make more fuel efficient engines(15). Since many of the parts will be unserviceable, the need exists for materials to withstand thermal cycling, and low expansion materials will be required. Other uses are catalyst supports, dimensionally stable optical supports, heat exchangers and many other applications which require low expansion materials(16).

Low thermal expansion materials may be classified into three groups. The first group consists of compounds with strong covalent bonding such as diamond(17). The second group includes glasses containing up to 85-100% SiO_2(except those such as alkali containing glasses). The low thermal expansion behavior exhibited by these systems may be due to bond angle bending and stretching during heating and to the high strength of the Si-O bond. Most low thermal expansion materials fall into the third group where the low expansion is due to the anisotropy of the crystal. These crystal systems include hexagonal(9,13), orthorhombic(10), monoclinic(18) and tetragonal (19).

The AV_2O_7 (A = Zr,Hf) compounds are cubic with a superstructure at room temperature that triples the ideal

unit cell. The thermal expansion behavior is determined to be isotropic, which would help in removal of micro cracks due to thermal cycling. In addition, the system is combined with AP_2O_7 to make a solid solution series where the thermal expansion coefficient, α, can be tuned to various values. The thermal expansion behavior and crystal structures are determined using high temperature X-ray diffraction (up to 250 °C), dilatometry (up to 850 °C) and Rietveld analysis using powder x-ray and neutron diffraction. This is presented in Chapter 6.

1.2 References

1. J. J. Brown and F. A. Hummel, *Trans. Brit. Ceramic Soc.*, **64, 419 (1965)**

2. F.R. Landsberg and P.J. Bray, *J. Chem. Phys.*, **53**, 2757 (1970)

3. G. Peyronel, *Gazz. Chim. Ital.*, **72**, 77 (1942)

4. D. F. Craig and F. A. Hummel, *J. Am. Ceram. Soc.*, **55**, 532 (1972)

5. F. A. Hummel, *Interceram*, **33[6]**, 27-30 (1984)

6. W. H. Dumbaugh, Jr., and J. W. Malmendier, "Refractory Glasses", *High Temperature Oxides, Part IV*, Academic Press, New York and London, 1-14 (1971)

7. M. E. Miolberg, and H. D. Blair, *J. Am. Ceram. Soc.*, **60[7-8]**, 372 (1977)

8. R. Roy, D.K. Agrawal, J. Alamo, and R. A. Roy, *Mat. Res. Bull.*, **19[4]**, 471-477 (1984)

9. J.S. Moya, A.G. Verduch and M. Hortal, *Trans. & Journ. of British Ceram. Soc.*, **73[6]**, 177 (1974)

10. C.E. Holcombe, Jr., *Am. Ceram. Soc. Bull.*, **59[12]**, 1219 (1980)

11. H.P. Kirchner, K. M. Merz, and W.R. Brown, *J. Am. Ceram. Soc.*, **46[3]**, 137 (1963)

12. K.R. Land, and F.A. Hummel, *J. Am. Ceram. Soc.*, **54[8]**, 407 (1971)

13. G.E. Lenain, H.A. Mckinstry, S.Y. Limaye, and A. Woodward, *Mat. Res. Bull.*, **19[11]**, 1451 (1984)

14. D.E. Harrison, H.A. Mckinstry, and F.A. Hummel, *J. Am. Ceram. Soc.*, **37[6]**, 277 (1954)

15. Gloria M. Caton et. al., "Ceramic Technology Newsletter", Ceramic technology project, Oak ridge national labs and Department of Energy under contract DE-AC05-84OR21400, January-March, No 42

16. Arden L. Bement, et. al.,"Materials and Processing Report", **4[3]**, June 1989

17. E. Bruton, "Diamonds", N.A.G. Press LTD., London, 300-307 (1970)

18. W.R. Manning, O. Hunter,Jr., F.W. Calderwood, and D.W. Stacy, *J. Am. Ceram. Soc.*, **55[7]**, 342 (1972).

19. W. Ostertag, G.R. Fischer, and J.P. Williams, *J. Am. Ceram. Soc.*, **51[11]**,651 (1968)

2. EXPERIMENTS AND SYSTEMS INVESTIGATED

2.1 Introduction

This chapter reviews the different systems investigated and some of the experiments that have been attempted during the course of my research. The systems explored are described along with the synthesis conditions. New compounds are identified.

2.2 Description of Reaction Systems

Several systems were investigated as shown in Table 2.1. Many different compositions within each system were tried using the starting materials shown in Table 2.2. A compound in the $Li/V^{V}/Bi/O$ system with the composition Li_2BiVO_5, showed an interesting feature in that at room temperature the material was yellow with small dark red spots, but upon heating to 100 °C the body color changed to a deep red. Attempts were made to synthesize single crystals using various temperature programs and different compositions. Typically the composition was A_2VBiO_x (A=Li,Na,K), and the reaction temperatures were raised to the melting point of the composition and slowly cooled to room temperature at a rate of 5 °C/hour. All attempts led

to a polycrystalline material with no single crystals suitable for structure analysis. Although no compound was found to have this composition in the JCPDS data file (1), a literature search revealed a Japanese patent describing a thermochromic temperature indicating material, whose composition was described as $BiVO_{4-x}M_2O$ (M = alkali metal; $x \leq 0.25$)(2). No US patents have been filed to date.

Table 2.1

Systems investigated

Systems	New Phases	Reaction Temperature °C
$Li/V^{V}/Bi^{III}/O$	Li_2VBiO_5	640 °C
	$Bi_4V_2O_{11}$	650 °C
$Na/V^{V}/Bi^{III}/O$	Na_2VBiO_5	640 °C
$K/V^{V}/Bi^{III}/O$	K_2VBiO_5	640 °C
$Li/V^{V}/P/O$	Li_2VPO_6	540 °C
$Na/V^{V}/P/O$	Na_2VPO_6	440 °C
$K/V^{V}/P/O$	K_2VPO_6	440 °C
$Rb/V^{V}/P/O$	None	~400 °C
$Li/V^{V}/Sn^{IV}/O$	None	~790 °C
$Li/V^{V}/Al/O$	None	~800 °C
$Li/V^{V}/B/O$	None	~800 °C
$Al/V^{V}/Bi^{III}/O$	$Bi_4V_2O_{11}$	~650 °C
$Sn^{IV}/V^{V}/Bi^{III}/O$	None	~650 °C
$Bi^{III}/V^{V}/B/O$	None	~800 °C

Table 2.1 (Continued)

$Zr/V^V/O$	ZrV_2O_7	800 °C
$Zr/V^V/P/O$	$ZrVPO_7$	800 °C
$Al/V^V/P/O$	None	~800 °C
$K/As/P/O$	None	~600 °C
$K/V^V/Pb/O$	None	~900 °C
$K/Pb/P/O$	$KPbPO_4$	700 °C
$Ca/V^V/B/O$	None	~780 °C
$K/V^V/Sb/O$	None	~500 °C
$Ca/V^V/P/O$	None	~900 °C
$Mg/V^V/P/O$	None	~900 °C

New Compounds were found in the $A/V^V/P/O$ (A=Li,Na and K) system were found; their synthesis, structures and properties are reported in chapters 3, 4 and 5. Investigation into the $Zr/V^V/P/O$ system led to new materials with interesting thermal expansion behavior which is described in Chapter 6.

Table 2.2

Reactants used in Synthesis

Compound	Manufacturer, purity
Li_2CO_3	Baker, Reagent
$LiNO_3$	Mallinckrodt, Reagent
Na_2CO_3	Mallinckrodt, Reagent
$NaNO_3$	Spectrum Chemical, Reagent
KNO_3	Mallinckrodt, 99.97%
$RbNO_3$	Johnson Matthey, 99.8%
NH_4VO_3	Johnson Matthey, 99%
$(NH_4)_2HPO_4$	Mallinckrodt, Reagent
Bi_2O_3	Atomergic Chemetals Corp., 99.9%
$Al(NO_3)_3 \cdot 9H_2O$	Baker, Reagent
SnO_2	Baker, Reagent
SnO	Baker, Reagent
H_3BO_3	Mallinckrodt, Reagent
$ZrOCl_2 \cdot 8H_2O$	Teledyne Wah Chang, Reagent
As_2O_5	Johnson Matthey, 99.99%
PbO	Aldrich, 99.9%
$Ca(NO_3)_2$	Baker, Reagent
Sb_2O_3	Baker, Reagent
MgO	Johnson Matthey, 98%

While investigating the $Al/V^V/Bi/O$ and $Li/V^V/Bi/O$ systems, yellow crystals were produced. The analysis of the structure of these crystals was attempted from X-ray diffraction data. The space group appeared to be $I\bar{4}$ (No.

82) with a = b = 3.927(8)Å and c = 15.418(3)Å, but a good refinement was not obtained. After more review of the literature, a compound with the composition Bi_2GeO_5 (3) was found with lattice constants of a = 15.69(7)Å b= 5.492(8)Å and c = 5.383(6)Å with a space group of $Cmc2_1$ (No. 36), suggesting a relationship to our yellow crystals. However, refinements with the Bi_2GeO_5 structure type failed, and no further work was performed. Later, reports were found that $Bi_4V_2O_{11}$ had similar cell dimension, but with both a and b doubled (4,5).

In the K/Pb/P/O system, a single phase material was found with the composition $KPbPO_4$. A search was conducted in chemical abstracts with nothing found for this composition. An indexing program called Visser was used to determine the lattice type for this material and subsequent lattice refinements were carried out as shown in Table 2.3. A search was made on this lattice type with the search software from Siemens and a close match with $KBaPO_4$ (6) was made. The literature search revealed the atomic coordinates as shown in Table 2.3.

Table 2.3

Lattice Parameters and Atomic Positions for $KPbPO_4$

$KPbPO_4$				$KBaPO_4$
System	Pnam (No. 62)			
a (Å) =	7.4463(8)			7.7084(5)
b (Å) =	9.959(2)			9.9783(8)
c (Å) =	5.6341(4)			5.6649(5)
V ($Å^3$)=	417.81			435.73
	x	y	z	
K	1/4	0.415	-0.330	
Ba	1/4	-0.312	0.000	
P	1/4	0.425	0.267	
O1	1/4	0.432	0.046	
O2	1/4	-0.417	0.350	
O3	0.005	0.343	0.337	

2.3 References

1. Powder Diffraction File, JCPDS International Centre for Diffraction Data, Swarthmore, PA

2. Takano Toshihiko, Yano Kozaburo, Kobayashi Yukiko, Inoue Yoshio, and Harada Shiegeo (Sharp Corporation) **Jpn. Kokai Yokkyo Koho JP 63 61,079; 63 61,080;** September 2, 1986

3. Bengt Aurivillius, Claes-Ivar Lindblom and Per Stenson, *Acta Chem. Scand.*, **18(6)**, 1555 (1964)

4. A. A. Bush., V. G. Koshelayeva and Yu. N. Venentsev, *Jap. J. Appl. Phys.*, **24(2)**, 625 (1985)

5. Wuzong Zhou, *J. Solid State Chem.*, **76**, 290 (1988)

6. C.W. Struck and J.G. White, *Acta Cryst.*, **15**, 290 (1962)

3. SYNTHESIS AND CRYSTAL STRUCTURE OF POTASSIUM AND SODIUM VANADIUM PHOSPHATES(1)

3.1 Introduction

Previous investigations of the K(I)/V(V)/P(V)/O system(2-5) have suggested compounds of the formulas KV_2PO_8, $K_4V_2P_4O_{17}$, $K_{11}V_3P_4O_{23}$, $K_3V_2PO_9$, K_2VPO_6, $K_6V_2P_2O_{13}$, $K_3V_8PO_{24}$, $K_3V_4P_2O_{14}$, $K_3V_2PO_9$ and $K_{24}V_2P_8O_{37}$. These should not all be regarded as firmly established discrete compounds. For example, the formulas given as $K_6V_2P_2O_{13}$ and $K_{11}V_3P_4O_{23}$ might really be the same phase. One may notice that in the list is a compound with the same generally formula as one of the title compounds, K_2VPO_6. This was synthesized in water free t-butanol by t-butyl potassium reacting with orthorhombic $KHVPO_6$.

$$K\text{-}O\text{-}C(CH_3)_3 + KHVPO_6 \rightarrow K_2VPO_6 + H\text{-}O\text{-}C(CH_3)_3$$

The compound was then dried under vacuum with P_2O_5 as a drying agent. This compound was amorphous as shown by powder x-ray diffraction and was very moisture sensitive, turning to a slurry in a matter of an hour. Upon putting it into water, there was a precipitate of $KHVPO_6$.

However, with K_2VPO_6 the compound simply dissolves and recrystallization does not occur.

A greater tendency for glass formation was observed for the Na(I)/V(V)/P(V)/O system, and only one compound, $Na_{12}V_3P_3O_{21}$, was reported(3456). If it were not for the potassium compound being discovered the sodium compound would have been missed, since the synthesis of this was attempted at an earlier date with only the formation of a glass. Structures were not reported for any of the previous known compounds in the K/V/P/O and Na/V/P/O systems. This chapter describes the synthesis of single crystals of K_2VPO_6 and Na_2VPO_6 and discusses details of the structures of these compounds.

3.2 Experimental

Yellow crystals of K_2VPO_6 were prepared by mixing NH_4VO_3 (Matthey Electronics, 99%), $(NH_4)_2HPO_4$ (EM Science, reagent), and KNO_3 (EM Science, reagent) in the molar ratios 1:1:2 respectively. After grinding in an agate mortar, the mixture was placed in a Pt crucible and heated at 50°C per hour to 350°C and held there for two hours to drive off ammonia and nitrate gases. The temperature was

then raised to 440°C; after holding for one hour, it was allowed to cool to room temperature at a rate of 10°C per hour. The same procedure was used for the sodium compound using $NaNO_3$ (Spectrum Chemical, reagent) in place of the KNO_3. Both compounds readily dissolve in water, and are not able to recrystallize in solution. The compounds were observed to be stable in air for at least several weeks.

Differential thermal analysis was carried out using a Netzsch STA 409 system. On heating K_2VPO_6 at 5°C/min., melting commenced at about 480°C. On cooling K_2VPO_6 at 5°C/min., crystallization occurred at 352°C. This is shown in Figure 3.1. Melting of Na_2VPO_6 occurred at 466°C, and recrystallization did not occur when cooling at a rate of 5°C/min. as shown in Figure 3.2. Infrared spectra of the compounds in KBr pellets were obtained on a Nicolet 5PC FTIR spectrometer.

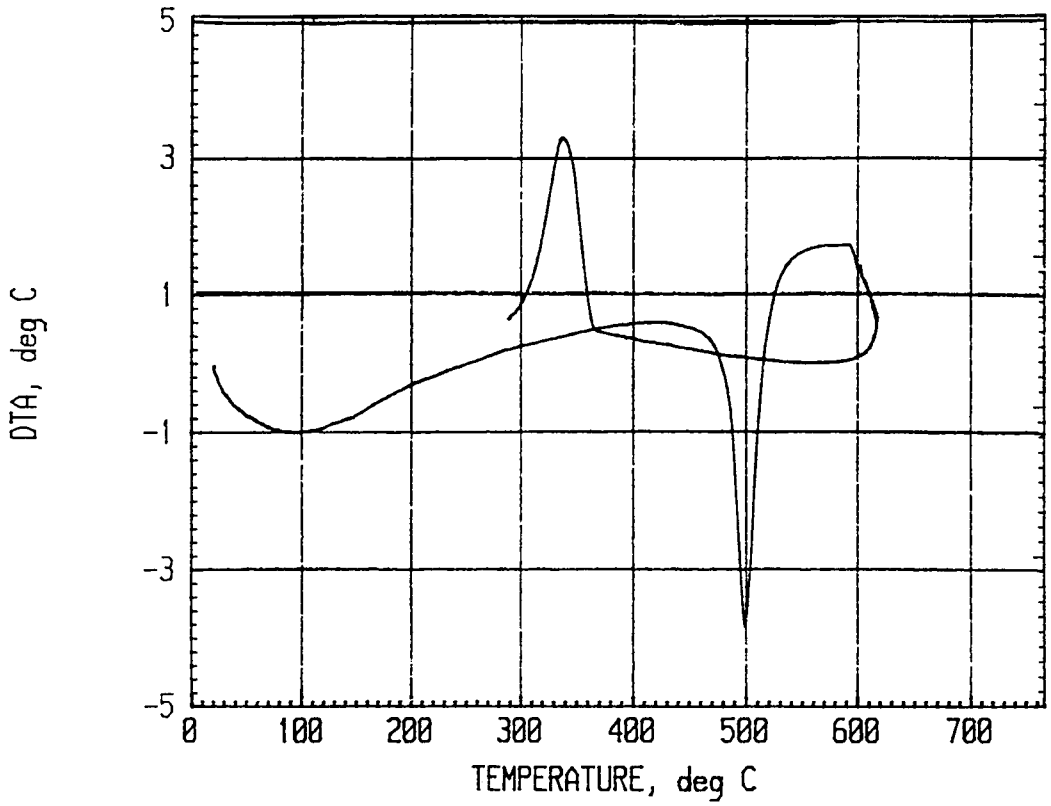

Figure 3.1 Differential Thermal analysis curve of K_2VPO_6. Endotherm peak on melting at 480 °C and an Exotherm peak at 352 °C.

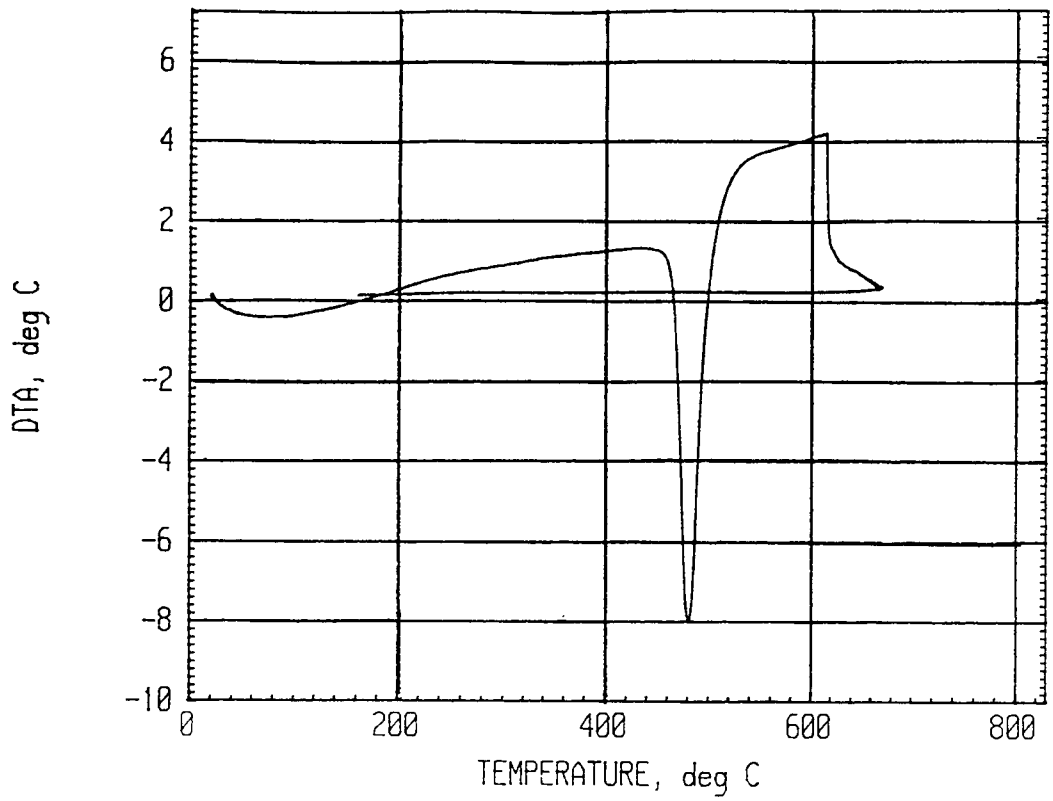

Figure 3.2 Differential Thermal Analysis curve of Na_2VPO_6. Endotherm peak on melting at 466 °C.

Crystals of dimensions 0.222 x 0.185 x 0.777 mm for K_2VPO_6 and 0.185 x 0.296 x 0.296 mm for Na_2VPO_6 were mounted on glass fibers for collection of single crystal X-ray diffraction data. Details of the data collection, reduction and refinement are summarized in Tables 3.1 and

3.2. The cell dimensions were refined by least squares refinement of 20 reflections that had been centered on a Rigaku AFC6R diffractometer. The intensities of three standard reflections measured every 300 reflections throughout the data collection exhibited no significant excursions. The structure was solved and refined with programs from the TEXAN crystallographic software package (7). The vanadium atoms were located by direct methods using SHELXS (8). The phosphorous, oxygen and alkali atoms were found in subsequent analysis of difference electron density maps. The final atomic position and isotropic thermal parameters are given in Tables 3.3 and 3.4. Anisotropic thermal parameters are given in Tables 3.5 and 3.6, and selected interatomic distances and angles are given in Tables 3.7 and 3.8.

Table 3.1

Crystal Data and Intensity Collection for K_2VPO_6

Empirical Formula	K_2VPO_6
Formula weight (g/mol)	256.11
Crystal System	Monoclinic
Space Group	$P2_1/n$ (no. 14)
a (Å)	6.863(2)
b (Å)	13.479(5)
c (Å)	7.505(1)
β (°)	111.02(1)
V ($Å^3$)	648.0(3)
Z	4
Diffractometer	Rigaku AFC6R
Radiation	Mokα (λ = 0.71069 Å) Graphite-monochromated
Temperature	23 °C
Maximum 2θ (°)	70
Data Collected	-11<h<11, 0<k<21, 0<l<13
Scan Speed (degrees/min)	16.0 in ω and 32.0 in 2θ
No. unique data with $Fo^2 > 3\sigma(Fo^2)$	2496
Data/parameter ratio	27.43
R	0.047
Rw	0.072

Table 3.2

Crystal Data and Intensity Collection for Na_2VPO_6

Empirical Formula	Na_2VPO_6
Formula weight (g/mol)	223.89
Crystal System	Monoclinic
Space Group	$P2_1/n$ (no. 14)
a (Å)	6.1805(7)
b (Å)	12.436(1)
c (Å)	7.386(1)
β (°)	107.00(1)
V ($Å^3$)	542.9(1)
Z	4
Diffractometer	Rigaku AFC6R
Radiation	Mokα (l = 0.71069 Å) Graphite-monochromated
Temperature	23 °C
Maximum 2θ (°)	120
Data Collected	-9<h<9, 0<k<20, -11<l<11
Scan Speed (degrees/min)	16.0 in ω and 32.0 in 2θ
No. unique data with $Fo^2 > 3\sigma (Fo^2)$	1447
Data/parameter ratio	16.07
R	0.030
Rw	0.045

Table 3.3

Atomic and Isotropic Thermal Parameters for K_2VPO_6

Atom	x	y	z	Beq(Å^2)*
V	0.29598(7)	0.20049(3)	0.90012(7)	1.25(1)
P	0.9247(1)	0.12171(5)	0.6971(1)	1.19(2)
K1	0.3617(1)	0.13192(5)	0.4469(1)	2.15(2)
K2	0.8050(1)	0.08066(5)	0.0893(1)	2.30(2)
O1	0.9862(3)	0.1958(1)	0.8661(3)	1.49(6)
O2	0.1469(3)	0.1044(2)	0.6907(3)	1.54(6)
O3	0.2801(4)	0.3283(2)	0.0117(3)	1.88(7)
O4	0.4593(4)	0.2349(2)	0.7969(4)	2.7(1)
O5	0.8250(4)	0.0291(2)	0.7339(3)	1.90(7)
O6	0.4230(4)	0.1281(2)	0.0763(3)	2.16(8)

* All atoms occupy site 4e in space group $P2_1/n$

** $Beq = (8\pi^2/3)\Sigma_i\Sigma_j U_{ij} a^*_i a^*_j a_i \cdot a_j$

Table 3.4

Atomic and Isotropic Thermal Parameters for Na_2VPO_6

Atom*	x	y	z	Beq(Å^2)**
V	0.28512(5)	0.21674(3)	0.8780	0.65(1)
P	0.90775(8)	0.11170(4)	0.69579(7)	0.63(2)
Na1	0.3213(2)	0.13985(8)	0.4245(1)	1.5(3)
Na2	0.8054(2)	0.07118(8)	0.0713(1)	1.72(3)
O1	0.9514(3)	0.1977(1)	0.8554(2)	0.81(4)
O2	0.1530(3)	0.1057(1)	0.6782(2)	1.11(5)
O3	0.2398(3)	0.3467(1)	0.0120(2)	0.96(5)
O4	0.4428(3)	0.2732(1)	0.7609(3)	1.43(6)
O5	0.8037(3)	0.0075(1)	0.7579(2)	1.21(5)
O6	0.4476(3)	0.1424(1)	0.0432(2)	1.48(6)

* All atoms occupy site 4e in space group P21/n

** $Beq = (8\pi^2/3)\Sigma_i\Sigma_j U_{ij} a^*_i a^*_j a_i \cdot a_j$

Table 3.5

Anisotropic Thermal Parameters (x 10^{-4} Å) For K_2VPO_6

Atom	U_{11}	U_{22}	U_{33}	U_{12}	U_{13}	U_{23}
V	177(2)	149(2)	184(2)	-5(2)	107(2)	-8(2)
P	181(3)	98(3)	204(3)	-7(2)	104(3)	1(2)
K(1)	390(4)	201(3)	311(4)	-122(3)	231(3)	-64(2)
K(2)	322(4)	239(3)	396(4)	70(3)	228(3)	60(3)
O(1)	191(9)	144(8)	270(10)	-8(7)	134(8)	-46(7)
O(2)	195(9)	193(9)	233(9)	-2(7)	122(7)	-60(8)
O(3)	230(10)	162(9)	300(10)	10(8)	71(8)	-56(8)
O(4)	370(10)	400(10)	370(10)	-170(10)	290(10)	-120(10)
O(5)	330(10)	133(8)	310(10)	-66(8)	170(10)	-5(8)
O(6)	300(10)	280(10)	260(10)	100(10)	120(10)	36(9)

Table 3.6

Anisotropic Thermal Parameters (x 10^{-4} Å) For Na_2VPO_6

Atom	U_{11}	U_{22}	U_{33}	U_{12}	U_{13}	U_{23}
V	65(2)	85(2)	96(2)	-1(1)	19(2)	-4(1)
P	85(2)	56(2)	92(2)	-1(2)	14(2)	-1(2)
Na1	185(5)	123(5)	270(5)	-47(3)	83(4)	-9(4)
Na2	197(5)	237(5)	223(5)	-91(4)	65(4)	-12(4)
O1	88(6)	103(6)	119(7)	0(5)	34(5)	38(5)
O2	199(6)	172(8)	149(7)	-5(6)	33(6)	75(6)
O3	114(7)	93(7)	130(7)	-3(5)	-7(5)	28(5)
O4	156(7)	216(8)	203(8)	39(7)	100(6)	7(7)
O5	204(7)	84(7)	155(7)	39(6)	28(6)	-27(6)
O6	159(8)	185(8)	189(8)	-68(6)	8(6)	-47(6)

Table 3.7

Bond Distances (Å) and Angles(°) for K_2VPO_6

V	O6	1.623(2)	P	O5	1.497(2)
	O4	1.642(2)		O3	1.545(2)
	O3	1.935(2)		O1	1.549(2)
	O2	2.010(2)		O2	1.561(2)
	O1	2.050(2)			
K1	O1	2.620(2)	K2	O6	2.667(3)
	O5	2.635(2)		O5	2.806(3)
	O2	2.756(2)		O5*	2.825(3)
	O3	2.788(3)		O1	2.873(2)
	O4	2.831(3)		O4	2.923(3)
	O6	2.959(3)		O2	2.944(2)
	O4*	3.144(3)			

O3-V-O2	145.1(1)	O6-V-O2	102.9(1)
O4-V-O1	143.5(1)	O3-V-O4	96.1(1)
O6-V-O1	108.2(1)	O4-V-O2	93.2(1)
O6-V-O4	107.2(2)	O3-V-O1	82.22(9)
O6-V-O3	106.2(1)	O1-V-O2	70.62(9)
O5-P-O2	113.4(1)	O1-P-O3	110.8(1)
O5-P-O1	113.3(1)	O5-P-O3	110.0(1)
O2-P-O3	110.9(1)	O2-P-O1	98.0(1)
O6-K1-O2	155.80(7)	O4-K1-O3	81.81(8)
O6-K1-O4	144.54(8)	O4-K1-O1	77.97(8)
O4-K1-O5	142.32(7)	O6-K1-O5	73.04(7)
O5-K1-O1	138.53(7)	O6-K1-O3	71.46(7)
O3-K1-O2	132.32(8)	O6-K1-O1	68.26(7)
O2-K1-O1	124.72(7)	O3-K1-O1	57.89(7)
O3-K1-O5	121.90(8)	O4-K1-O2	56.97(7)
O2-K1-O5	87.37(7)		
O5*-K2-O6	148.13(7)	O4-K2-O5*	95.85(8)
O2-K2-O1	143.11(6)	O1-K2-O5*	93.01(7)
O4-K2-O5	125.84(7)	O4-K2-O6	88.80(8)
O2-K2-O4	118.38(7)	O5*-K2-O5	88.55(8)
O1-K2-O6	118.34(7)	O4-K2-O1	72.64(7)
O5-K2-O6	114.03(8)	O1-K2-O5	53.21(6)
O2-K2-O5	106.80(7)	O2-K2-O5*	52.55(6)
O2-K2-O6	97.73(7)		

Table 3.8

Bond Distances (Å) and Angles(°) for Na_2VPO_6

V	O6	1.624(2)	P	O5	1.498(2)
	O4	1.638(2)		O3	1.538(2)
	O3	1.957(2)		O1	1.556(2)
	O2	2.011(2)		O2	1.561(2)
	O1	2.034(2)			
Na1	O1	2.287(2)	Na2	O6	2.3348(2)
	O5	2.305(2)		O4	2.394(2)
	O2	2.432(2)		O5	2.438(2)
	O3	2.482(2)		O5*	2.494(2)
	O4	2.539(2)		O1	2.583(2)
	O4*	2.897(2)		O2	2.838(2)
	O6	3.135(2)			

O2-V-O3	148.23(6)	O2-V-O6	100.94(8)
O4-V-O1	138.78(8)	O4-V-O3	96.23(7)
O1-V-O6	112.63(7)	O4-V-O2	94.78(7)
O4-V-O6	107.95(9)	O1-V-O3	81.14(6)
O3-V-O6	103.80(7)	O1-V-O2	71.06(6)
O2-P-O5	112.8(1)	O1-P-O5	111.27(9)
O3-P-O5	111.65(9)	O1-P-O3	111.13(8)
O2-P-O3	111.33(9)	O1-P-O2	97.95(8)
O4*-Na1-O5	156.22(6)	O4-Na1-O2	84.20(6)
O4-Na1-O3	147.15(7)	O4-Na1-O5	84.20(6)
O1-Na1-O5	132.97(7)	O4-Na1-O1	81.53(6)
O1-Na1-O2	125.71(7)	O4*-Na1-O3	75.46(6)
O2-Na1-O3	117.34(7)	O4*-Na1-O1	70.48(6)
O3-Na1-O5	114.94(7)	O1-Na1-O3	65.84(6)
O4*-Na1-O5	97.82(5)	O4*-Na1-O2	60.07(5)
O2-Na1-O5	96.81(7)		
O5-Na2-O6	154.73(7)	O1-Na2-O5	97.38(6)
O1-Na2-O2	153.32(6)	O5*-Na2-O6	93.11(6)
O4-Na2-O5*	133.78(7)	O4-Na2-O6	84.83(7)
O5*-Na2-O6	110.66(7)	O4-Na2-O5	84.62(7)
O2-Na2-O5*	109.92(6)	O4-Na2-O1	74.97(6)
O4-Na2-O2	107.24(7)	O1-Na2-O5*	59.51(5)
O2-Na2-O6	104.74(6)	O2-Na2-O5	57.15(5)
O1-Na2-O6	101.95(7)		

3.3 Discussion

The structures of K_2VPO_6 and Na_2VPO_6 are shown in Figures 3.3 and 3.4. The structures contain the same

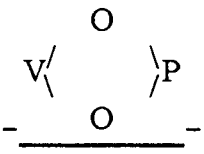

-O- helical chains shown in Figure 3.5. The square pyramidal vanadium polyhedra share one edge (O1 and O2) and one corner (O3) with a phosphorous tetrahedron leaving two terminal oxygens (O4 and O6) on vanadium and one (O5) on the phosphorous. The bonds to all terminal oxygens are shorter as would be expected. The angle between the edge sharing polyhedra is also very small due to the repulsion between the vanadium and the phosphorous atoms (Tables 3.7, 3.8).

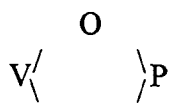

The -O- chains are all parallel to one another, and an array of these chains is shown in Figure 3.6. As might be expected of an array of parallel chains, the chains tend to be hexagonally close packed. However, several factors necessarily destroy the true hexagonal symmetry. The chain axis itself does not possess symmetry

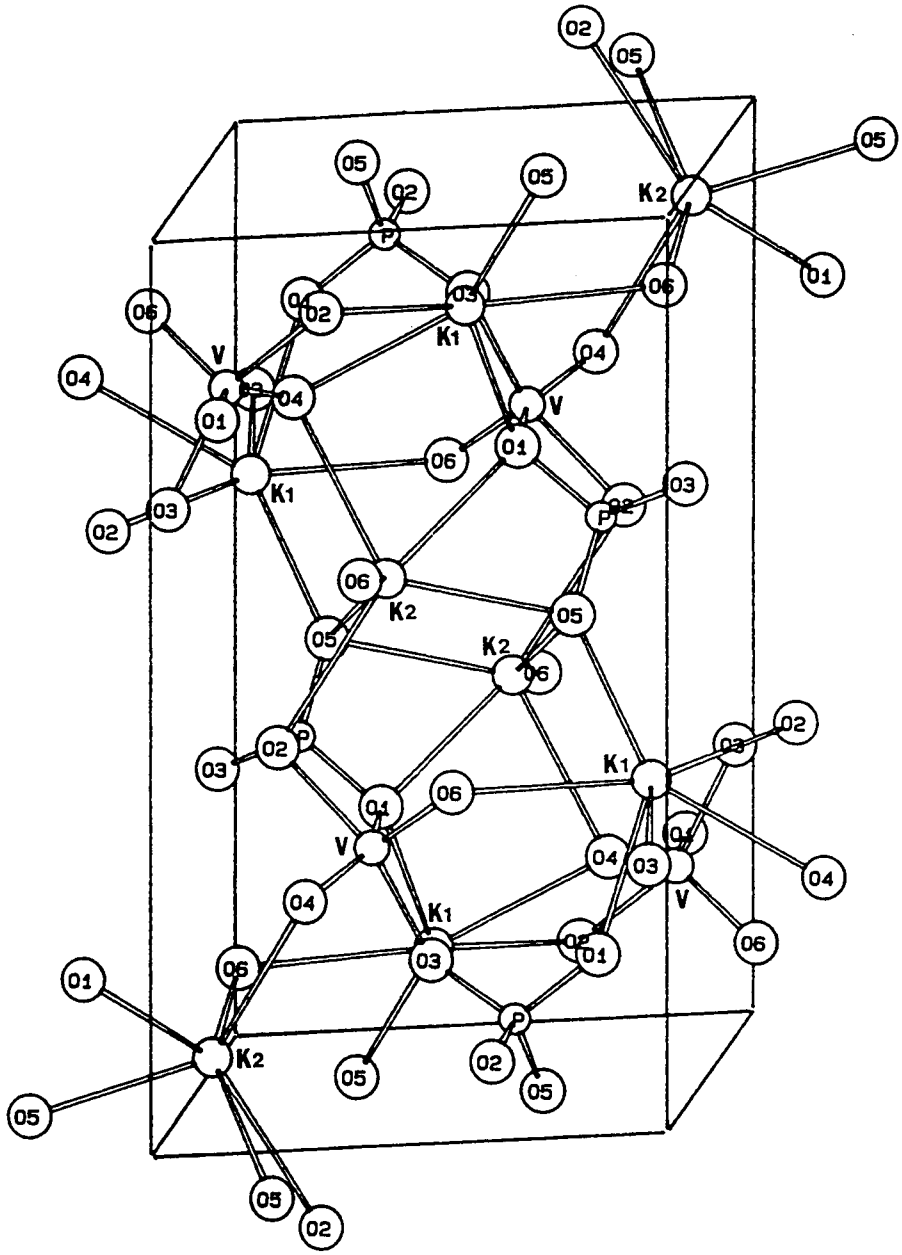

Figure 3.3 Unit cell of K_2VPO_6 showing complete polyhedra of cations.

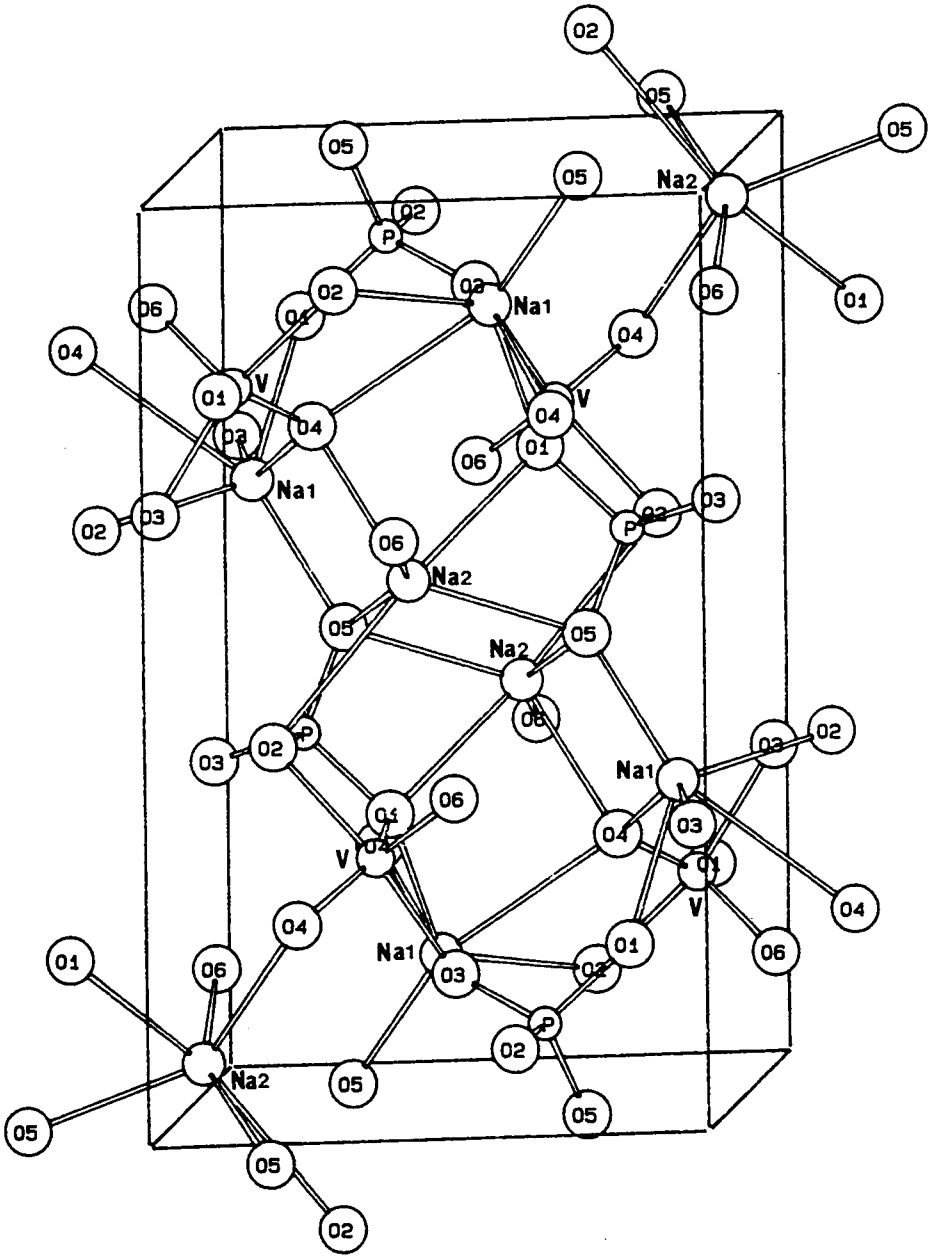

Figure 3.4 Unit cell of Na_2VPO_6 showing complete polyhedra of cations.

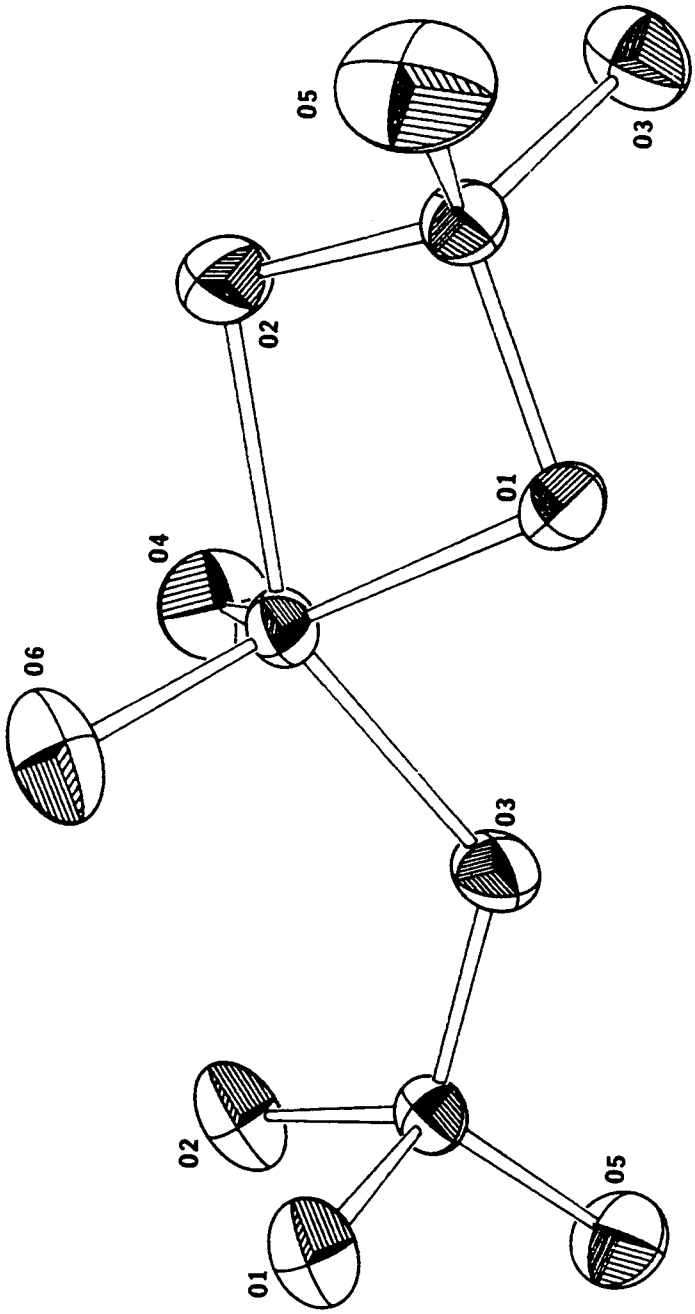

Figure 3.5 Chain structure for both K_2VPO_6 and Na_2VPO_6.

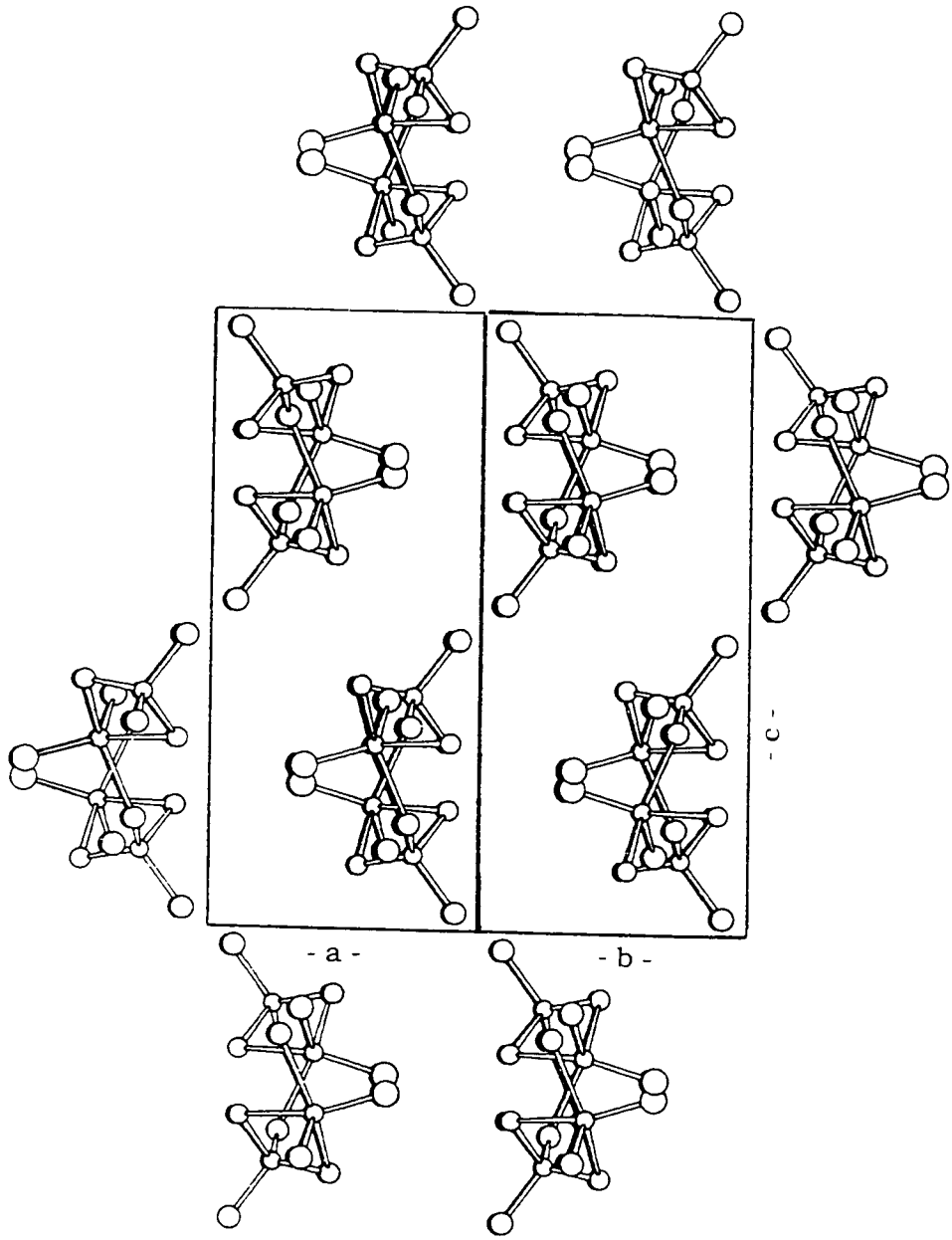

Figure 3.6 View down the 101 plane of K_2VPO_6 perpendicular to the $-VO_2PO-$ chains. Large circles represent oxygen atoms. Each chain in this projection shows two vanadium atoms near the center of the chain and two phosphorous atoms further out.

approaching a six-fold axis. Furthermore, the chains may be considered as arrows which point up or down due to the n-glide plane and the 2_1 Screw axis. Looking at Figure 3.6, one can imagine that all the chains that are running at 1/4 of the c-axis are rows of alternating up and down arrows due to the n-glide plane, bringing one chain closer to the viewer than its neighbor. The screw axis turns the chain 180° perpendicular to its axis and translates it up to 3/4 of the c-axis. Thus if one is looking at an up arrow and it is operated on by the screw axis it remains an up arrow because it is not projected away from the viewer. The arrows are of course further apart in K_2VPO_6 than in Na_2VPO_6 due to larger ionic radii of the potassium ions. The center-to-center distances for arrows pointing in one direction is 6.557Å and 7.099Å for Na_2VPO_6 and K_2VPO_6, respectively. The center-to-center distances for arrows pointing in opposite directions is 5.465Å and 5.924Å for Na_2VPO_6 and K_2VPO_6, respectively. Thus, oppositely pointing arrows are closer to each other, but all arrows are a little more than eight percent further apart in the potassium compound. The chains are also stretched in K_2VPO_6 relative to Na_2VPO_6. Taking the cation-cation distances along the chain as the indicator

of stretching, one concludes that this stretching is about three percent. Bond distances have not changed significantly, but several of the bond angles have changed significantly. There is one atom in this chain (O3) which has a coordination number of only two, neglecting coordination to the alkali cations. Thus, this bond angle (V-O3-P) can readily change to compress or expand the chain length. This angle increases by about seven degrees (124.4° to 131.3°) on going from Na_2VPO_6 to K_2VPO_6. The opening up of this angle is the primary factor in stretching the chain. These distances and angles are summarized in Table 3.9.

All the alkali cations in Na_2VPO_6 to K_2VPO_6 might be described as six coordinated to oxygen. However, the coordination in all cases is highly irregular. Thus, designating a specific coordination number is somewhat arbitrary. It is interesting to note that the six oxygens closest to Na1 are not the same as the six oxygens closest to K1 (Tables 3.7 and 3.8).

The infrared spectra for Na_2VPO_6, K_2VPO_6, and Li_2VPO_6 (9) are shown in Figure 3.7 with suggested band assignments in Table 3.10 (10,11,12). As expected, the spectra for Na_2VPO_6 and K_2VPO_6 are essentially the same

because they contain essentially identical 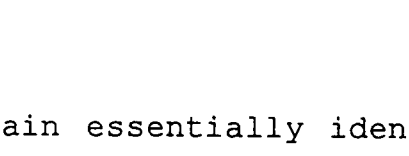 chains. As shown in the next chapter, the Li_2VPO_6 structure on the other hand has sheets with octahedrally coordinated vanadium and a very different infrared spectrum. Also shown in figure 3.7 are the infrared spectra of glasses of the composition Na_2VPO_6 and K_2VPO_6. These spectra are essentially broadened spectra of their crystalline analogs. We can assume that these glasses contain segments of the same chains found in crystalline Na_2VPO_6 and K_2VPO_6.

Table 3.9

Distances and angles in the

-VOPO- chain and distances between chains

	K_2VPO_6	Na_2VPO_6
V-V	4.2896(8)	4.1470(8)
V-P*	2.6751(7)	2.6685(6)
V-P	3.1752(7)	3.0977(6)
P-P	5.346(1)	5.3239(9)
V-O3-P	131.3(1)	124.40(9)
P-V-P	131.88(2)	134.69(2)
V-P-V	93.93(2)	91.67(2)
V-V-V	143.74(2)	156.99(2)
P-P-P	99.39(2)	99.51(2)
P-V-V*	157.11(1)	149.37(2)
P-V-V	108.25(2)	119.40(2)
V-P-P*	112.54(2)	106.14(2)
V-P-P	87.22(2)	92.55(2)

Chain distances due to

Screw Axis	Glide plane	Screw Axis	Glide plane
7.0992(5)	5.9240(8)	6.5569(5)	5.4647(7)

Edge sharing connection (e.g. P-V-V; P-V corner connection; V* is the next Vanadium (opposite direction) through the edge connection P)

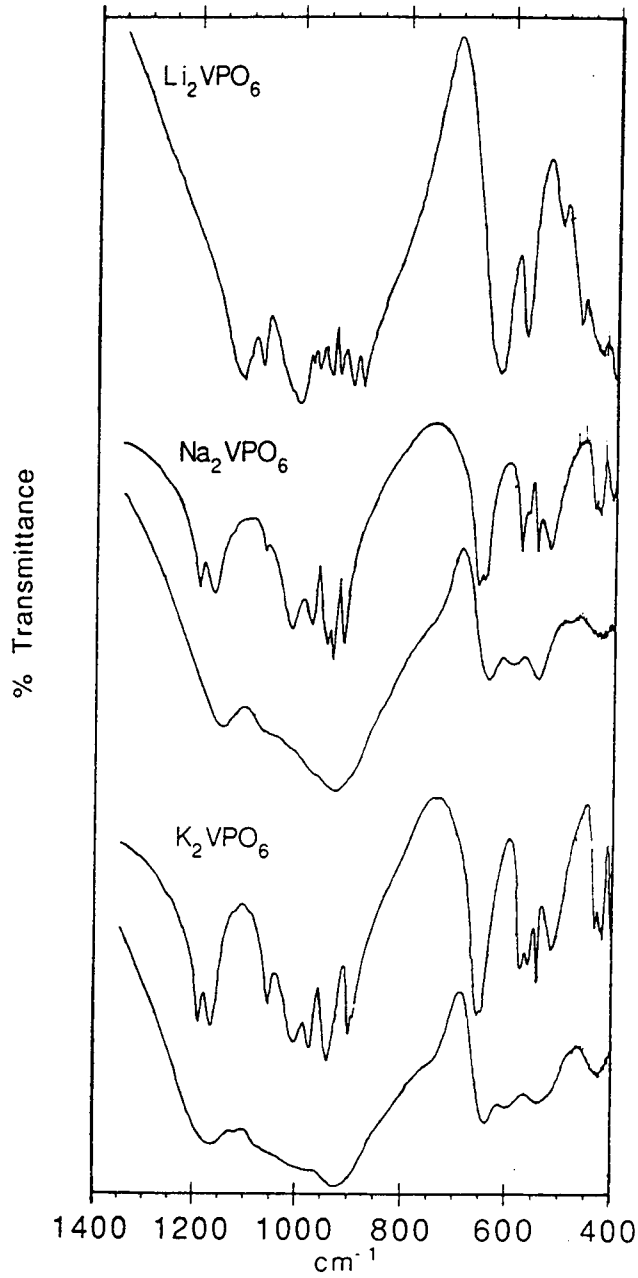

Figure 3.7 IR spectra of Li_2VPO_6, K_2VPO_6 and Na_2VPO_6. Below the spectra of the crystalline Na and K compounds are the spectra of the glass analogs of the same composition.

Table 3.10

IR Peak Wavenumbers (cm^{-1}) and Empirical Assignments

K2VPO6	Na2VPO6	Li2VPO6	
cm^{-1}	cm^{-1}	cm^{-1}	Assignments
1191	1195		
1167	1166	1112	ν_{as} P-O
1057	1067	1075	
1005	1014	1019	
		1002	V=O Stretch
974	975	977	
939	947	967	
	934	941	
899	916	926	ν_{s} P-O Stretch
892		902	
		882	
655	660	623	δ_{as} O-P-O
648	647	616	
575	578	572	
560			δPO + δVO
546	549		
518	524	507	
436	439	470	
420	427	427	δ_{s} O-P-O
400	404		

3.4 References

1. V.C. Korthuis, R.D. Hoffmann, Jinfan Huang and A.W. Sleight, Chemistry of Materials, **5(2)**, 206, 1993

2. V.V. Illarionov, R.P.Ozerov and E.V. Kil'disheva, *Russ. J. Inorg. Chem.*, **5**(12), 1352 (1960).

3. A.G. Bergman and Z.I. Sanzharova, *Russ.J. of Inorg. Chemistry*, **15**(6), 877-878 (1970)

4. A.G. Bergman and Z.I. Sanzharova, *Russ. J. of Inorg. Chem.*, **15**(4), 581-582 (1970)

5. Fritz Preuss and Heinrich Schug, *Z. Naturforsh. 30 b*, 334-339 (1975)

6. V. V. Illarionov, A.I. Soklakov, and E.V. Kil'disheva, *Russ. J. of Inorg. Chem*, **6**(6), 696-699, (1961)

7. *TEXSAN*, Molecular Structure Corporation, The Woodlands, TX , USA (1988).

8. *Crystallographic Computing 3*; Eds. G. M. Sheldrick, C. Kruger, and R. Goddard, Oxford University Press, 1985, pp. 175-189.

9. V. Korthuis, R.D. Hoffmann, Jinfan Huang and A.W. Sleight, *J. Solid State Chem.*, **105**, 294-299 (1993)

10. R.N. Bhargava and A. Condrate SR., *Applied Spectroscopy*, **31**(3),230-236 (1977)

11. E. Bordes and P. Courtine, *Journal of Catalysis*, **57**, 236-252 (1979)

12. R. D. Hardcastle, Ph.D. Thesis, Lehigh University (1990)

4. SYNTHESIS AND CRYSTAL STRUCTURE OF A NEW LAYERED PHOSPHATE, Li_2VPO_6 (1)

4.1 Introduction

Phase diagram studies have not been reported for the Li/V(V)/P(V)/O system, and apparently no compounds are known which contain these four elements. I investigated the Li/V/P/O system under conditions where one would expect vanadium and phosphorous to be fully oxidized. Thus, one may consider this to be the three component system: $Li_2O/P_2O_5/V_2O_5$. The only compound I have found that contains substantial quantities of the three components is the title compound Li_2VPO_6. As mentioned previously in Chapter 3, the isostructural compounds Na_2VPO_6 and K_2VPO_6 which have analogous formulas, have a distinctly different structure than that which is reported here for Li_2VPO_6.

4.2 Experimental

Reactants used were $LiNO_3$ (Mallinckrodt, reagent), NH_4VO_3 (Matthey Electronics, 99%), and $(NH_4)_2HPO_4$ (EM Science, reagent). Various mixtures were ground together

and heated in air using platinum crucibles. The synthesis temperature ranged from 500 to 650°C; some melting normally occurred at the higher temperature. Light yellow crystals of Li_2VPO_6 were found in samples where melting had occurred. Along with the Li_2VPO_6 crystals, the X-ray powder diffraction always showed some LiV_3O_8 and Li_3PO_4 in such products, even for the 2Li:1V:1P stoichiometry. However, LiV_3O_8 could be removed by dissolving in 30% H_2O_2, and Li_3PO_4 was a fine powder which could be separated from the Li_2VPO_6 crystals using sieves.

A crystal of dimensions 0.063 x 0.188 x 0.313 mm was mounted on a glass fiber for collection of single crystal X-ray diffraction data. Details of the data collection, reduction and refinement are summarized in Table 4.1. The cell dimensions were refined by least squares refinement of 25 reflections in the range 28° to 30° 2 θ that had been centered on a Rigaku AFC6R diffractometer. A total of 1090 reflections were collected using the ω-2θ scan technique at a scan width of $(1.63 + 0.3 \tan \theta)°$. The intensities of three standard reflections measured every 300 reflections throughout the data collection exhibited

Table 4.1

Crystal Data and Intensity Collection for Li_2VPO_6

Empirical Formula	Li_2VPO_6
Formula weight (g/mol)	191.79
Crystal System	Orthorhombic
Space Group	$Pna2_1$ (no. 33)
Lattice parameter from single crystal	
a (Å)	10.314(2)
b (Å)	4.6328(6)
c (Å)	8.562(1)
V ($Å^3$)	409.1(1)
Lattice parameter from powder diffractometer	
a (Å)	10.3219(3)
b (Å)	4.6355(1)
c (Å)	8.5620(4)
V ($Å^3$)	409.69(2)
Z	4
Diffractometer	Rigaku AFC6R
Radiation	Mok_α (λ = 0.71069 Å) Graphite-monochromated
Temperature	23 °C
Maximum 2θ (°)	70
Data Collected	$0<h<14$, $0<k<17$, $0<l<7$
Scan Speed (degrees/min)	16.0 in ω and 32.0 in 2θ
No. unique data with $F_o^2 > 3\sigma(F_o^2)$	763
Data/parameter ratio	8.38
R	0.041
R_w	0.046

no significant excursions. An empirical absorption correction was made using psi scan data which resulted in transmission factors ranging from 0.65 to 1.0 with an average of 0.91. The structure was solved and refined with programs from the TEXSAN crystallographic software package (2). The vanadium atoms were located by direct methods using SHELXS (3). The phosphorous, oxygen and lithium atoms were found in subsequent analysis of difference electron density maps. The structure was refined by full matrix least squares cycles. Atomic scattering factors (4) were corrected for anomalous dispersion (5). The weighting scheme was based on the counting statistics, and a factor accounting for secondary extinction was refined and applied to the calculated structure factors. A final residual of R = 0.041 was obtained using anisotropic thermal parameters for 763 structure factors and 91 variables. Refinement in the enantiomorph setting resulted in a R-value slightly higher (R= 0.042). The acentric space group was confirmed by showing second harmonic generation when using a YAG:Nd laser (1/3 that of KTP).

X-ray diffraction powder patterns were obtained on a Siemens D5000 diffractometer using Cu $K\alpha$ radiation and Si(a = 5.43094 Å) as an internal standard. The cell dimensions were refined by least squares, and they are in good agreement with those obtained from the four circle

diffractometer (Table 4.1). An indexed powder X-ray diffraction pattern for Li_2VPO_6 is listed in Table 4.2. Intensity calculations (6) based on the positional parameters of the refined structure facilitated the identification of diffraction lines.

The final atomic position and isotropic thermal parameters are given in Table 4.3. Anistropic thermal parameters are given in Table 4.4, and selected interatomic distances and angles are given in Table 4.5.

Differential thermal analysis was carried out using a Netzsch STA 409 system. A freshly prepared powder of Li_2VPO_6 was used for the DTA run. Incongruent melting of Li_2VPO_6 commenced at about 545°C as shown in Figure 4.1. After the run, powder X-ray diffraction showed Li_3PO_4 and LiV_3O_8. The LiV_3O_8 phase is black and is most likely oxygen deficient, i.e., LiV_3O_{8-x}. The Li_3PO_4 phase can be seen as dark green crystals. Polycrystalline Li_2VPO_6 may be prepared single phase by carrying out the synthesis below 545°C. However, then crystals are not obtained.

Table 4.2

Observed and calculated values for d-spacing and Intensity

dcalc	dobs	Icalc	Iobs	hkl	dcalc	dobs	Icalc	Iobs	hkl
5.1611	5.1630	14	28	200	1.6921	-	1	-	314
4.4202	4.4193	100	100	201	1.6904	-	1	-	421
4.2811	4.2820	15	9	002	1.6867	1.6865	1	1	601
4.2287	4.2284	35	36	110	1.6475	1.6477	2	1	404
4.0764	4.0744	11	10	011	1.6253	1.6253	8	4	205
3.7915	3.7882	49	51	111	1.6129	-	<1	-	610
3.4487	3.4461	4	4	210	1.6063	-	<1	-	015
3.2950	3.2935	34	25	202	1.5995	1.5999	11	8	422
3.1989	3.1979	13	14	211	1.5963	-	1	-	602
3.0085	3.0086	56	42	112	1.5944	1.5948	3	3	323
2.7628	2.7618	1	2	310	1.5872	-	<1	-	115
2.6857	2.6836	1	1	212	1.5850	1.5849	2	2	611
2.6293	2.6288	45	48	311	1.5734	-	<1	-	513
2.5805	2.5799	1	2	400	1.5725	1.5725	5	4	024
2.4976	2.4979	5	5	203	1.5545	1.5546	1	1	124
2.4708	2.4713	6	6	401	1.5524	1.5528	1	1	414
2.4303	-	1	-	013	1.5416	1.5414	1	2	520
2.3656	2.3653	26	18	113	1.5338	-	<1	-	215
2.3214	2.3204	13	9	312	1.5281	-	1	-	130
2.3178	-	1	-	020	1.5206	1.5207	1	1	031
2.2614	2.2610	5	4	120	1.5172	1.5169	2	2	521
2.2547	2.2552	16	17	410	1.5093	-	<1	-	612
2.2100	2.2094	9	7	402	1.5044	-	1	-	131
2.1987	2.1987	30	25	213	1.5042	1.5040	3	2	224
2.1865	-	1	-	121	1.4803	-	<1	-	230
2.1804	2.1810	2	2	411	1.4759	-	2	-	423
2.1405	2.1399	4	2	004	1.4734	1.4733	16	8	603
2.1143	-	<1	-	220	1.4586	1.4586	2	1	231
2.0527	2.0524	9	7	221	1.4555	1.4555	10	4	315
2.0382	2.0384	4	3	022	1.4504	-	<1	-	522
1.9996	2.0000	6	4	122	1.4392	1.4391	1	1	132
1.9949	-	<1	-	412	1.4302	-	<1	-	324
1.9851	1.9845	5	3	313	1.4270	1.4271	9	3	006
1.9772	1.9761	2	1	204	1.4268	-	1	-	405
1.9223	1.9223	4	3	320	1.4150	1.4152	5	3	514
1.9141	1.9137	5	4	403	1.4096	1.4097	1	1	330
1.9098	1.9100	8	4	114	1.4052	1.4051	1	1	400
1.8957	1.8952	1	1	222	1.4042	-	<1	-	613
1.8859	1.8862	8	8	510	1.3990	1.3987	1	1	232
1.8756	-	1	-	321	1.3908	1.3907	4	2	331
1.8417	1.8417	3	2	511	1.3867	1.3867	4	2	711
1.8187	1.8189	2	1	214	1.3814	-	<1	-	620
1.7725	1.7721	<1	1	123	1.3754	-	1	-	206
1.7692	-	<1	-	413	1.3652	-	<1	-	125
1.7536	-	<1	-	322	1.3637	1.3636	3	2	621
1.7258	-	4	-	512	1.3588	-	1	-	415
1.7243	1.7246	11	6	420	1.3564	-	<1	-	033
1.7204	1.7205	3	4	600	1.3521	-	<1	-	523

Table 4.3

Atomic and Isotropic Thermal Parameters for Li_2VPO_6

Atom	x	y	z	Beq(Å^2)*
V	0.60978(8)	0.0169(2)	0	0.57(3)
P	0.2181(1)	0.0854(3)	0.8041(2)	0.55(4)
Li1	0.411(1)	0.519(2)	0.821(1)	1.2(4)
Li2	0.363(1)	0.035(3)	0.122(1)	1.8(5)
O1	0.2803(5)	0.193(1)	0.6506(5)	0.6(1)
O2	0.0818(4)	0.2316(8)	0.8114(6)	0.7(1)
O3	0.7160(4)	0.7409(8)	0.8139(6)	0.8(1)
O4	0.2857(4)	0.237(1)	0.9419(5)	0.7(1)
O5	0.4888(4)	0.7963(9)	0.9732(5)	0.7(1)
O6	0.5478(5)	0.241(1)	0.1272(5)	0.9(2)

* $B_{eq} = (8\pi^2/3)\Sigma_i\Sigma_j U_{ij} a^*_i a^*_j a_i a_j$

Table 4.4

Anisotropic Thermal parameters (x 10^{-4} Å) for Li_2VPO_6

ATOM	U11	U22	U33	U12	U13	U23
V	59(3)	91(4)	65(3)	-8(4)	3(4)	11(4)
P	75(5)	63(6)	72(5)	-1(5)	8(6)	-4(6)
Li(1)	140(10)	130(10)	190(10)	-5(4)	1(4)	2(5)
Li(2)	280(10)	300(10)	8(5)	2(6)	1(5)	3(5)
O(1)	110(10)	5(2)	8(2)	-1(2)	1(2)	-1(1)
O(2)	8(2)	5(2)	140(10)	1(1)	-1(2)	-2(2)
O(3)	140(10)	4(2)	110(10)	1(2)	-3(2)	-3(2)
O(4)	110(10)	6(2)	9(2)	-1(2)	-1(1)	-1(1)
O(5)	6(2)	8(2)	140(10)	-2(1)	-2(1)	-1(1)
O(6)	140(10)	110(10)	9(2)	1(2)	-1(2)	-3(2)

Table 4.5
Bond Distances (Å) and Angles(°) for Li_2VPO_6

V	O5	1.629(4)	P	O3	1.514(4)
	O6	1.633(5)		O4	1.539(5)
	O1	1.973(4)		O1	1.545(5)
	O2	2.012(5)		O2	1.563(4)
	O4	2.202(5)			
	O3	2.318(5)			
Li1	O5	2.00(1)	Li2	O4	1.97(1)
	O6	2.04(1)		O3	2.11(1)
	O4	2.11(1)		O5	2.13(1)
	O2	2.11(1)		O6	2.13(1)
	O3	2.30(1)		O1	2.18(1)
	O1	2.50(1)		O2	2.22(1)

O3-V-O6	173.2(2)	O1-V-O6	95.9(2)
O4-V-O5	157.7(2)	O1-V-O4	85.9(2)
O1-V-O2	153.2(2)	O3-V-O5	85.4(2)
O1-V-O5	102.9(2)	O1-V-O3	84.6(2)
O5-V-O6	101.1(2)	O2-V-O3	80.6(2)
O4-V-O6	98.3(2)	O3-V-O4	75.0(2)
O2-V-O5	98.1(2)	O2-V-O4	68.7(2)
O2-V-O6	96.4(2)		
O3-P-O4	114.8(3)	O1-P-O4	108.5(2)
O2-P-O3	114.7(2)	O1-P-O2	105.6(3)
O1-P-O3	112.0(3)	O2-P-O4	100.4(2)
O2-Li1-O3	174.1(6)	O3-Li1-O5	93.3(5)
O1-Li1-O5	170.9(6)	O2-Li1-O5	92.5(5)
O4-Li1-O6	149.7(6)	O1-Li1-O6	88.1(5)
O4-Li1-O5	109.1(6)	O3-Li1-O6	84.0(4)
O2-Li1-O4	101.0(5)	O1-Li1-O3	78.7(4)
O1-Li1-O2	95.5(4)	O3-Li1-O4	77.1(4)
O5-Li1-O6	95.4(5)	O1-Li1-O4	65.2(3)
O2-Li1-O6	95.4(5)		
O2-Li2-O4	167.0(7)	O2-Li2-O6	92.2(5)
O3-Li2-O5	163.4(7)	O4-Li2-O5	91.5(5)
O1-Li2-O6	158.2(7)	O1-Li2-O3	90.3(5)
O3-Li2-O4	102.7(6)	O2-Li2-O5	87.2(5)
O4-Li2-O6	99.7(6)	O2-Li2-O3	80.8(4)

Table 4.5 (Continued)

O1-Li2-O4	99.0(6)	O5-Li2-O6	72.6(5)
O3-Li2-O6	96.3(6)	O1-Li2-O2	68.3(4)
O1-Li2-O5	95.9(6)		

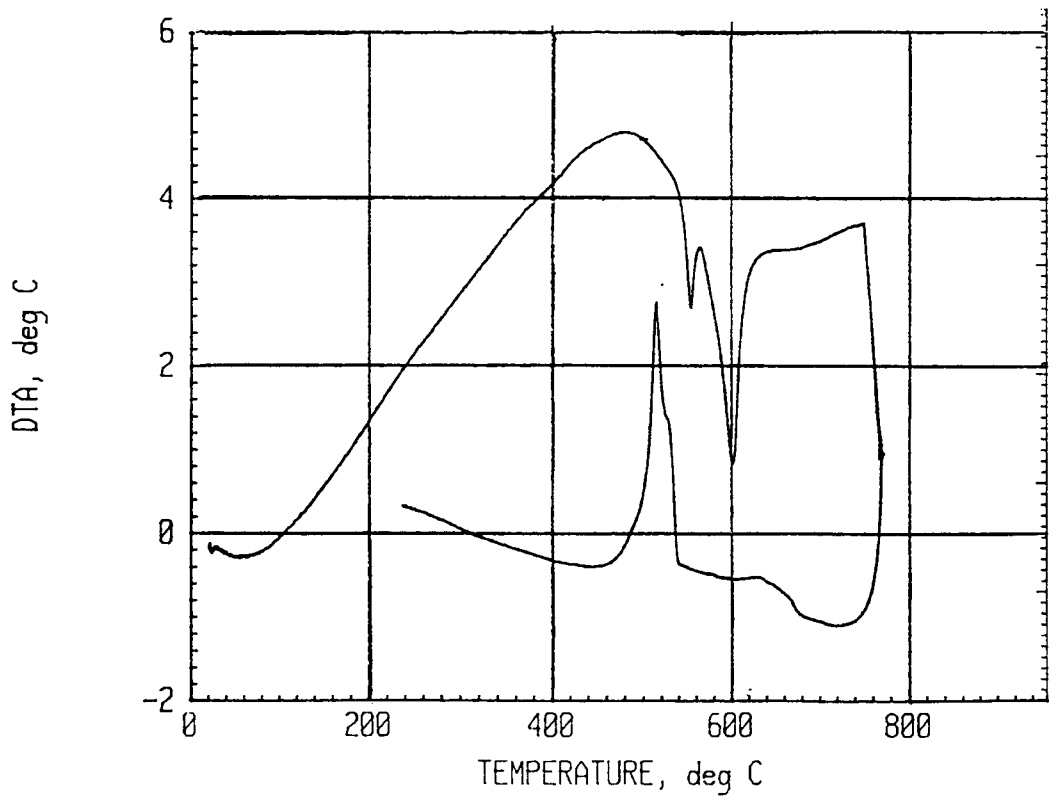

Figure 4.1 Differential Thermal Analysis (DTA) of Li_2VPO_6.

4.3 Discussion

The structure of Li_2VPO_6 may be considered as phosphate tetrahedra and vanadate octahedra linked to form a covalently bonded layer (Fig. 4.2) with an overall negative charge which is balanced by lithium cations between the layers. The layer is composed of interconnecting six membered rings of vanadium octahedra and phosphorous tetrahedra shown more detailed in Figure 4.3.

The lithium coordination is irregular (Fig. 4.3) as might be expected in such a situation, but both lithium cations can be viewed as six coordinated to oxygen (Table 4.5). In this description, most of the oxygen atoms have a coordination number of four, but O5 and O6 have a coordination number of only three. The average Li-O distance for Li2 is 2.12Å whereas the average Li-O distance for Li1 is 2.18Å. The significantly longer average distance for Li1 is consistent with the greater distortion of the Li1 octahedron. In fact, if the two long Li1-O bonds are eliminated, one may describe Li1 as in distorted tetrahedral coordination with an average Li-O

distance of 2.06Å. If this view is adopted, the coordination numbers for O1 and O3 also drop to three.

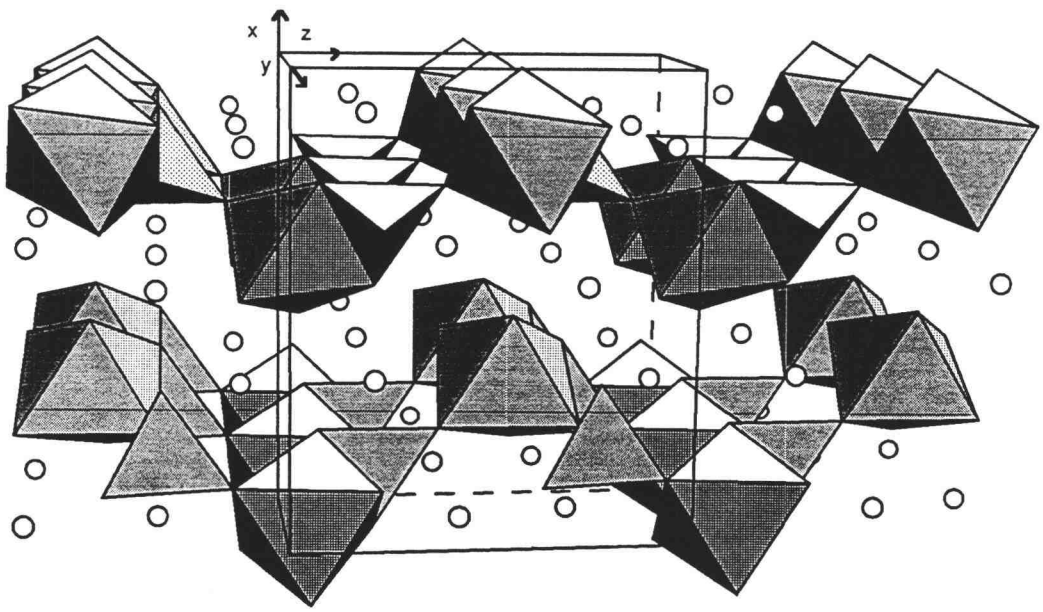

Figure 4.2 Layered structure of Li_2VPO_6. Small open circles represent lithium cations between layers of vanadium octahedra and phosphorous tetrahedra.

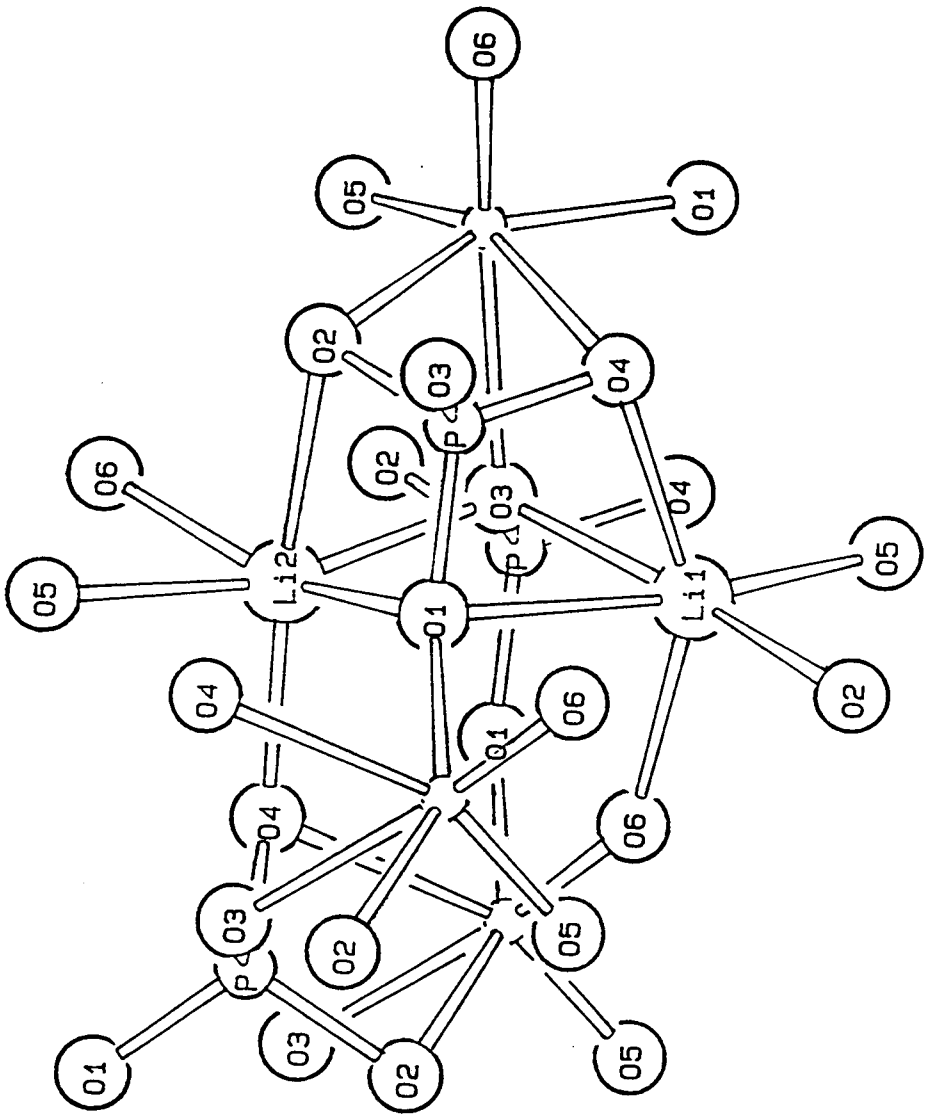

Figure 4.3 Vanadium-oxygen-phosphorous ring, showing the lithium coordination.

The coordination of vanadium to oxygen is distorted octahedral (Fig. 4.4) typical of pentavalent vanadium. The two short vanadium oxygen bonds (O6,O5) cause much of the distortion. As one might expect, the two short bonds are never observed to be trans to one another due to competing overlap with the vanadium d-orbitals. This in turn causes longer vanadium oxygen bonds trans to these vanadyl bonds. To date this is one of the only observed V(V) phosphates to have two short vanadium oxygen bonds. Most typically one finds one short vanadium oxygen bond as in α-VPO_5 (7), β-VPO_5 (8) and in V_2O_5 (9). These may be described either as square pyramidal vanadium or octahedral chains of vanadium with alternating long short bonds.

Also in this structure there is an unusual sharing of the vanadium octahedron with the edge of the phosphate tetrahedron. This leads to an additional distortion caused by the repulsion between vanadium and phosphorous across this edge. The O2-V-O4 angle of this edge is only 68.7°, considerably smaller than the ideal octahedral value. Likewise, the O2-P-O4 angle for this edge is only 100.4°, much smaller than the ideal tetrahedral value.

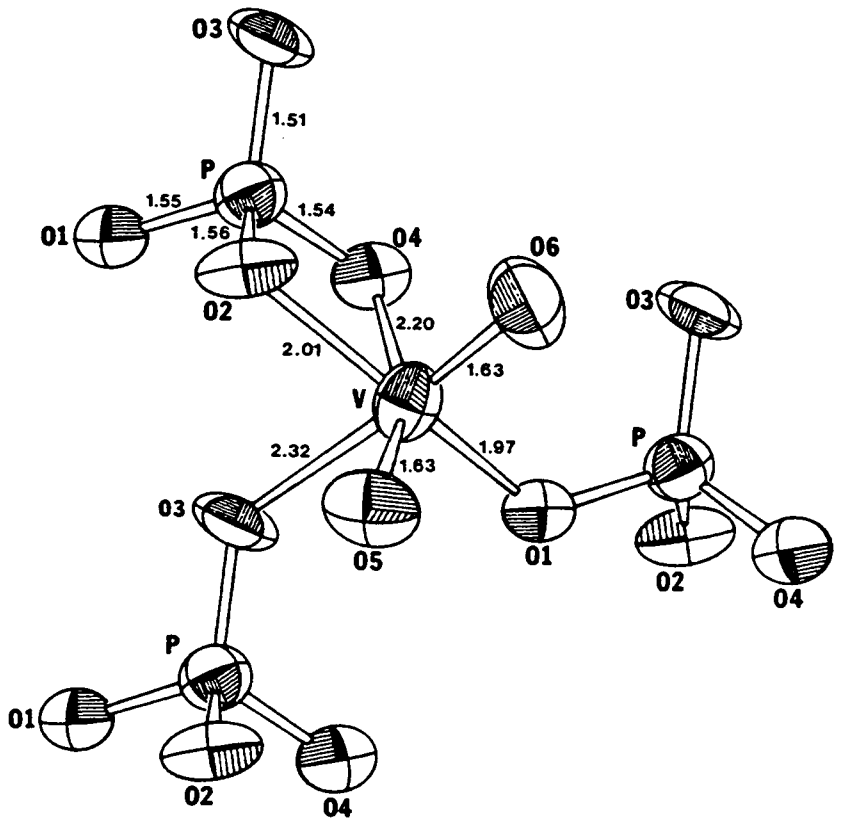

Figure 4.4 The environment of vanadium and phosphorous in Li_2VPO_6.

4.4 References

1. V.C. Korthuis, R.D. Hoffmann, Jinfan Huang, and A.W. Sleight, *J. Solid State Chemistry*, **105**, 294, (1993)

2. *TEXSAN*, Molecular Structure Corporation, The Woodlands, TX , USA (1988).

3. *Crystallographic Computing 3*, Eds. G. M. Sheldrick, C. Kruger, and R. Goddard, Oxford University Press, 1985, pp. 175-189.

4. Cromer, D.T., Mann, J.B., *Acta Crystallogr.*, Sect. A, **24**, 321, (1968).

5. Cromer, D.T. Liberman, D., *J. Chem. Phys.*, **53**, 1891, (1970).

6. K. Yvon, W. Jeitschko, and E. Parthe, *J. Appl. Cryst.* **10**, 73 (1977).

7. B. Jordan and C. Calvo, *Canad. J. Chem.*, **51**, 2621 (1973)

8. R. Gopal and C. Calvo, *J. Solid State Chem.*, **5**, 432 (1972)

9. H. G. Bachmann, F.R. Ahmed, and W.Z. Barnes, *Z. Kristallogr.*, **115**, 110 (1961)

5. IONIC CONDUCTIVITY OF Na_2VPO_6, K_2VPO_6 AND Li_2VPO_6.

5.1 Introduction

For any material and charge carrier, the specific conductivity, σ, is given by

$$\sigma = \Sigma\, n_i e_i u_i$$

where n_i is the number of charge carriers of species i, e_i is their charge and u_i is their mobility. The conductivity follows an Arrhenuis type behavior such that

$$\sigma = A \exp^{-(E_a/RT)}$$

where E_a is the activation energy, R is the gas constant and T is the temperature in Kelvins and A is the prefactor term which contains several constants, including the vibrational frequency of the potentially mobile ions. If one has the conductivity values at a series of temperatures, a plot of $\log_e \sigma$ versus 1/T will give a straight line of slope -E/R. In some treatments a reciprocal temperature term is included in the prefactor, A, in which case, it is normal to plot $\log_e \sigma T$ against T^{-1} (1). This will make a small difference to the value of the slope -E/R.

Measurements of accurate conductivity values, especially in polycrystalline samples, is often quite difficult due to an added resistance between grains (R_{gb}).

Ideally, the direct current (d.c.) conductivity should be measured, in order to be sure that the values pertain to long range ion migration and not to dielectric losses associated for example with rattling of ions within cages. The problem with d.c. measurements is finding electrode materials compatible with the solid electrolyte under study. One would like electrodes that can act as a source and a sink for the mobile ions, be easy to work with and able to withstand a wide thermal range.

Using blocking electrodes, which are electrodes that do not allow the migrating ions of the electrolyte to migrate and discharge into the electrodes, one would encounter problems associated with ions piling up on one electrode surface and an ion depletion at the other electrode surface. This is termed double layer capacitance (C_{dl}). Since d.c. methods measure current as a function of voltage, or vice versa, the current would initially be very high and would fall exponentially with time due to the build up of ions repelling each other at the electrode surface.

The alternative to d.c. methods is to use alternating current (a.c.) over a wide range of frequencies. The advantage in using a.c. techniques is that it enables one to separate out bulk and interfacial responses as well as intergranular resistance and capacitance (C_{gb}) using simple blocking electrodes such as gold and platinum.

Some of the disadvantages include knowledge of a.c. theory, and at high frequency (e.g. > 20 Mhz) lead problems occur and at the low frequency (e.g. < 10 mHz) cycle times become very long.

When a varying voltage is applied across a conductor, one must not only consider the change in current, but also the reaction of the conductor to the variation in current. For example, the quantity of charge (Q) stored in a capacitor depends on the voltage across the capacitor V_c:

$$Q = C\ V_c$$

If the voltage V_c varies with time, we see there must be a change in the charge Q, and therefore a current is required. Since current is the rate of charge flow, the current required is directly proportional to the rate of change in the voltage. Therefore the voltage cannot change instantaneously because it would require an infinite amount of current. For a.c. signals the term impedance, Z (ohms), is defined to take this effect into account. The a.c. methods of determining electrical conduction in solids has been termed impedance spectroscopy.

In a.c. measurements, the current and voltage are not in phase across a capacitor and thus an alternative approach is to represent the resistance or impedance as a sum of the imaginary and real components as (2)

$$Z^* = Z' - jZ''$$

where $j = \sqrt{-1}$, Z' is the real and Z'' is the imaginary component. In order to provide information about a particular system, a model using equivalent circuits is used to provide a description of the response generated. The most common being a resistor and capacitor in parallel to one another, representing the bulk resistance and the bulk capacitance. Since in parallel, resistors add as 1/R and capacitors add as $j\omega C$ ($\omega = 2\pi f$), one can solve for the real and imaginary components as

$$Z' = R_b/(1+(\omega R_b C_b)^2) \text{ and } Z'' = R_b \left[\omega R_b C_b / (1 + (\omega R_b C_b)^2) \right]$$

Where $R_b = \ell/A\sigma$ and $C_b = \varepsilon_o \varepsilon_r A/\ell$

ℓ = electrolyte thickness (cm)

A = electrolyte area (cm^2)

σ = electrolyte conductivity (Ω^{-1} cm^{-1})

ε_o = permittivity of a vacuum (F cm^{-1})

ε_r = dielectric constant of the electrolyte (F cm^{-1})

Therefore one can plot Z' vs. Z'' and obtain the true bulk resistance of the material on the Z' axis as shown in Figure 5.1. This type of plot is very useful in separating out the bulk resistance from grain boundary resistances if the capacitances are different. A typical situation for blocking electrodes is shown in Figure 5.2. For every parallel RC circuit one gets a semi-circle to represent it, provided the capacitances are somewhat different. Some typical values for capacitances are given in Table 5.1. There are many ways to represent the same

data using different formalisms related to impedance. These are summarized in Table 5.2 and the reader is encouraged to read the references for a detailed discussion of their uses (3, 4,5).

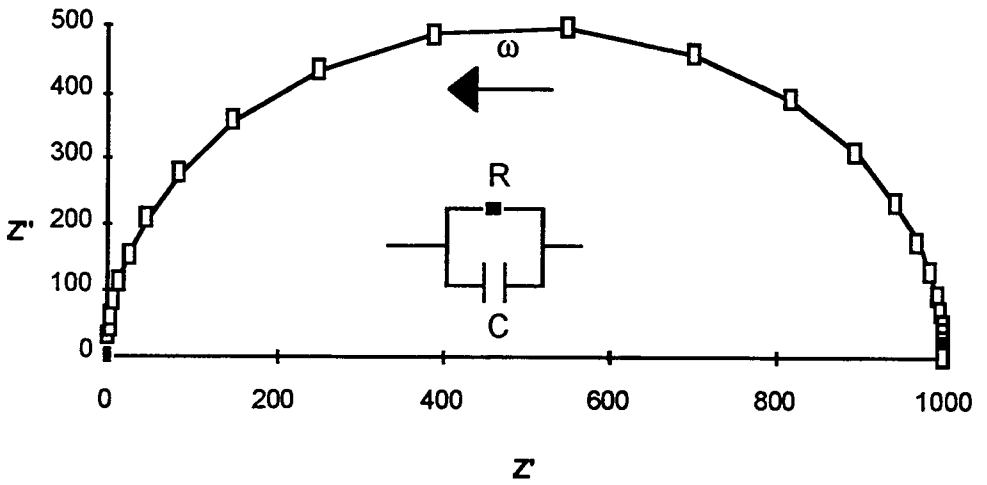

Figure 5.1. Cole-cole plot using non-blocking electrodes. R_b = 1000 Ω, C_b = 1 x 10^{-12} F. The point of the semicircle touchdown is R_b.

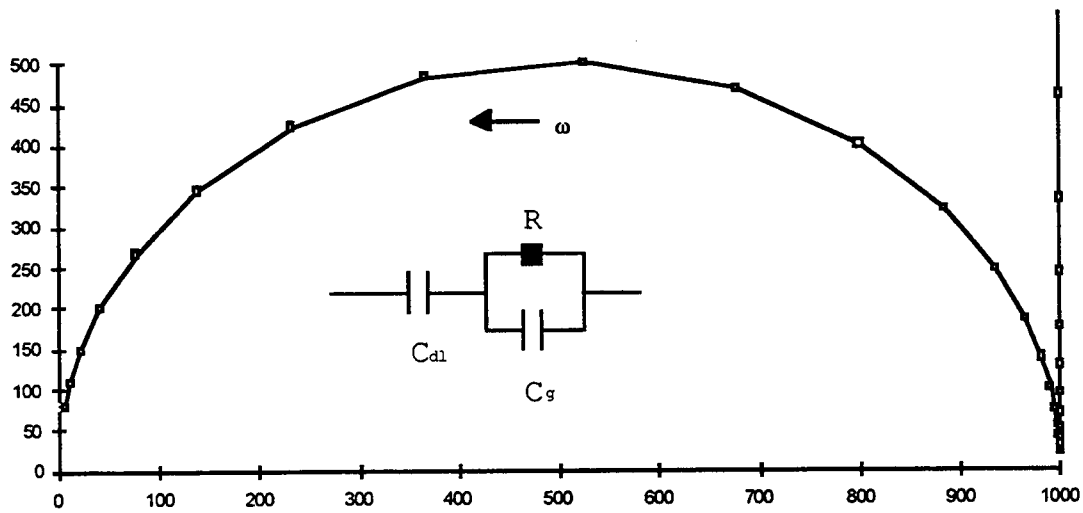

Figure 5.2 Cole-cole plot using blocking electrodes. R_b = 1000 Ω, C_b = 1 x 10^{-12} F, C_{dl} = 5 x 10^{-6} F.

Table 5.1

Typical values for types of capacitance

C_{dl}	1-50 μF
C_{gb}	1-100 nF
C_b	1-10 pF

Table 5.2

Complex Formalisms used in Impedance Spectroscopy

Formalism	Highlights
Complex Impedance (Z^*)	Capacitance differs Shows resistances
Complex Modulus (M^*)	Resistances differ Shows Capacitances
Complex Admittance (Y^*)	Frequency independent R
Complex Permittivity (ε^*)	Frequency independent C

5.2 Experimental

Details of the preparation of the A_2VPO_6 (A=Li,Na,K) samples are given in the preceding chapters. The bulk samples were ground in an agate mortar, then pressed in pellets of varying thickness with a diameter of 1/2" (1.27 cm). The pellets were then sintered in a furnace up to 400°C. Then a gold paste (Engelhardt, conductor composition) was applied to both surfaces and heated to 400 °C to drive off the organics. Measurements were made on a Solatron 1260 impedance analyzer computer controlled over the frequency range of 15 Mhz to 1 mHz using platinum electrodes. An impedance cell was constructed as shown in Figure 5.3, to allow for a closed atmosphere and to reach temperatures in excess of 600°C using our existing furnace. Temperature stabilization was maintained for approximately 40 minutes before a measurement took place.

5.3 Results

A pellet of Na_2VPO_6 with a length of 2.08 mm was run at a series of temperatures as shown by the complex

impedance spectrum in Figure 5.4. From the complex impedance spectrum the bulk resistances were determined and conductivities were calculated as shown in Table 5.3. The activation energy was determined by least squares, and is shown in Figure 5.5. The activation energy was calculated to be 73.6 Kcal/Mole at the higher temperatures and 28.3 Kcal/Mole at the lower temperatures.

A pellet of K_2VPO_6 with a length of 1.06 mm was run at a series of temperatures. Bulk resistances were determined as above and conductivites were calculated and are shown in Table 5.4. The activation energy was determined to be 26.0 KCal/Mole at the lower temperatures and 34.1 KCal/Mole at the higher temperatures from Figure 5.6.

The Li_2VPO_6 sample was pressed into a pellet with a length of 1.06 mm. It was measured at a series of temperatures where bulk resistances and conductivites were determined as above and are shown in Table 5.5. The activation energy was determined from Figure 5.7 to be 30.0 KCal/Mole.

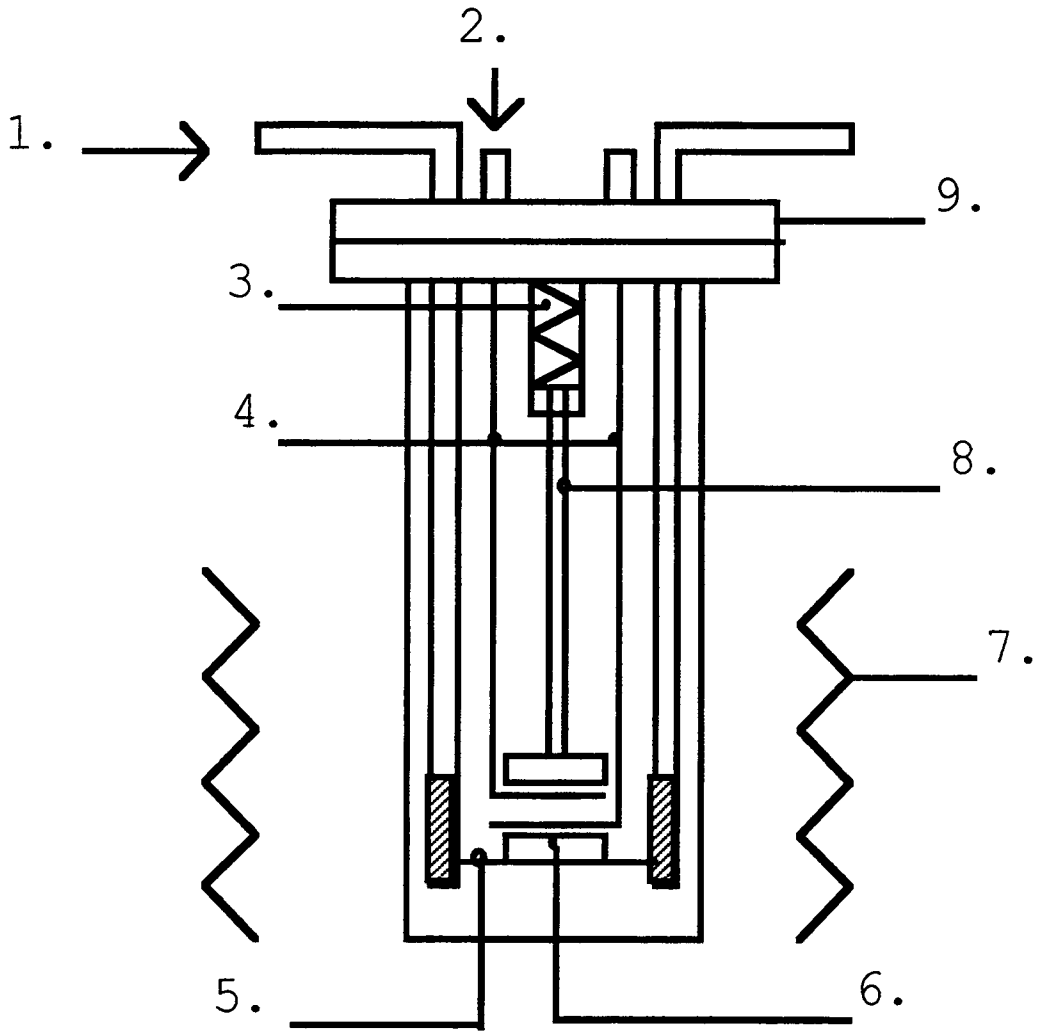

Figure 5.3 Impedance Cell used in high temperature measurements. (1) Hollow Stainless steel tubes, threaded on bottom to move stage (5). (2) BNC Connectors on top of Flange (9). (3) Spring to push down rod (8). (4) Platinum wires leading down to platinum foil on top of machinable ceramic (6). (7) Heating elements of furnace.

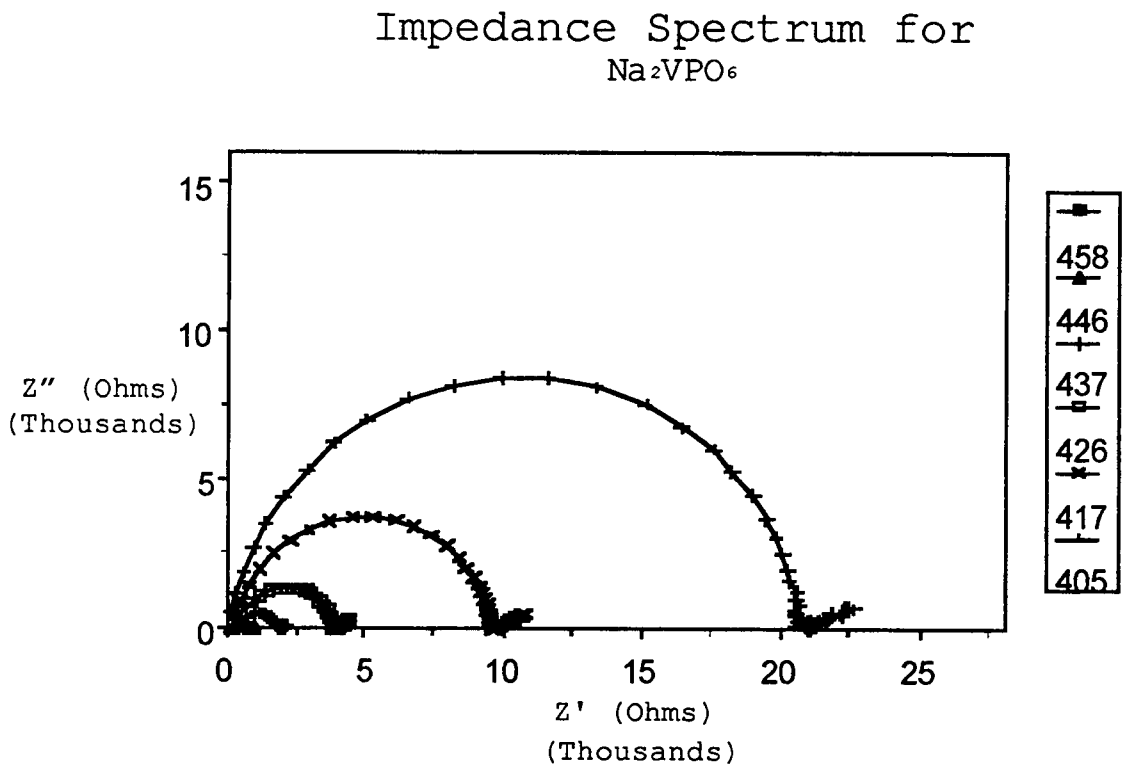

Figure 5.4 Complex Impedance spectrum of Na_2VPO_6 at a series of temperatures.

Table 5.3

Impedance Data for Na_2VPO_6

Temperature (°C)	Resistance (Ω)	Conductivity (Ω^{-1} cm^{-1})
458	213	7.71×10^{-4}
446	793	2.07×10^{-4}
437	1840	8.92×10^{-5}
426	3860	4.25×10^{-5}
417	9650	1.70×10^{-5}
405	21000	7.82×10^{-6}
396	38200	4.30×10^{-6}
384	65300	2.51×10^{-6}
378	194000	8.46×10^{-7}
366	290000	5.66×10^{-7}
354	435000	3.77×10^{-7}
345	658000	2.50×10^{-7}
334	995000	1.65×10^{-7}
323	1520000	1.08×10^{-7}
313	2300000	7.14×10^{-8}
301	3470000	4.73×10^{-8}

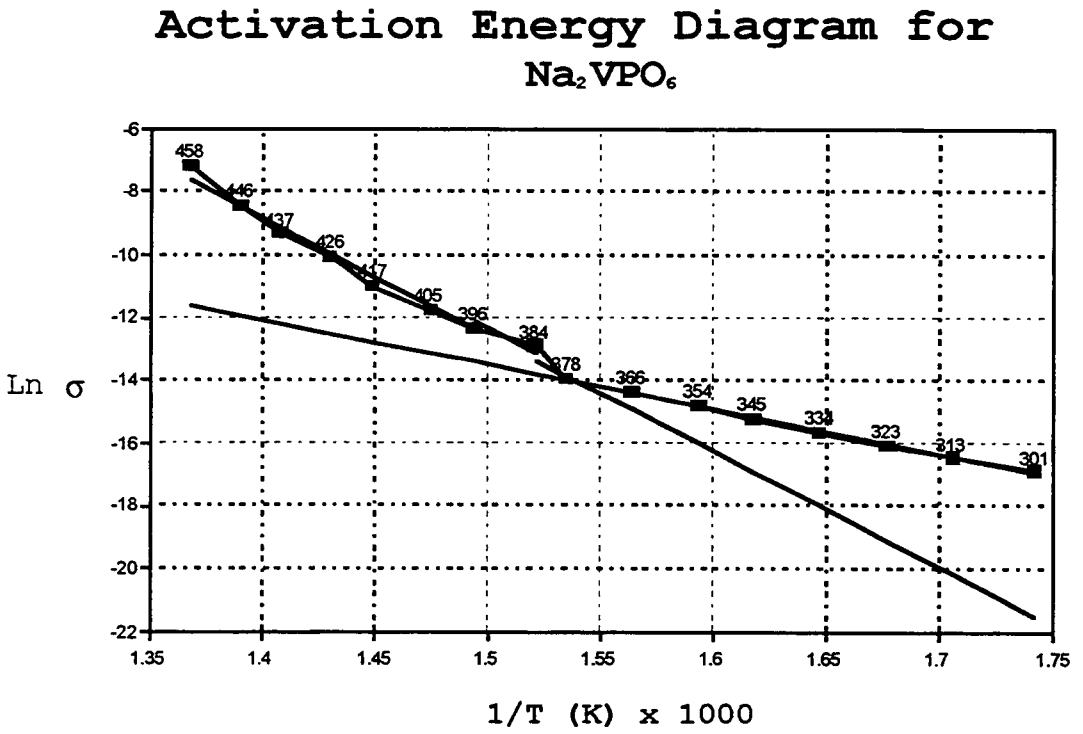

Figure 5.5 Activation Energy Diagram for Na_2VPO_6.

Table 5.4

Impedance Data for K_2VPO_6

Temperature (°C)	Resistance (Ω)	Conductivity (Ω^{-1} cm^{-1})
440	5310	3.94×10^{-6}
434	6330	3.30×10^{-6}
425	9840	2.13×10^{-6}
413	14500	1.44×10^{-6}
404	20700	1.01×10^{-6}
395	29000	7.21×10^{-7}
383	40800	5.13×10^{-7}
377	50800	4.12×10^{-7}
366	77000	2.72×10^{-7}
354	107000	1.96×10^{-7}
345	151000	1.39×10^{-7}
333	216000	9.68×10^{-8}
324	311000	6.73×10^{-8}
312	455000	4.60×10^{-8}
303	674000	3.10×10^{-8}
294	1000000	2.09×10^{-8}

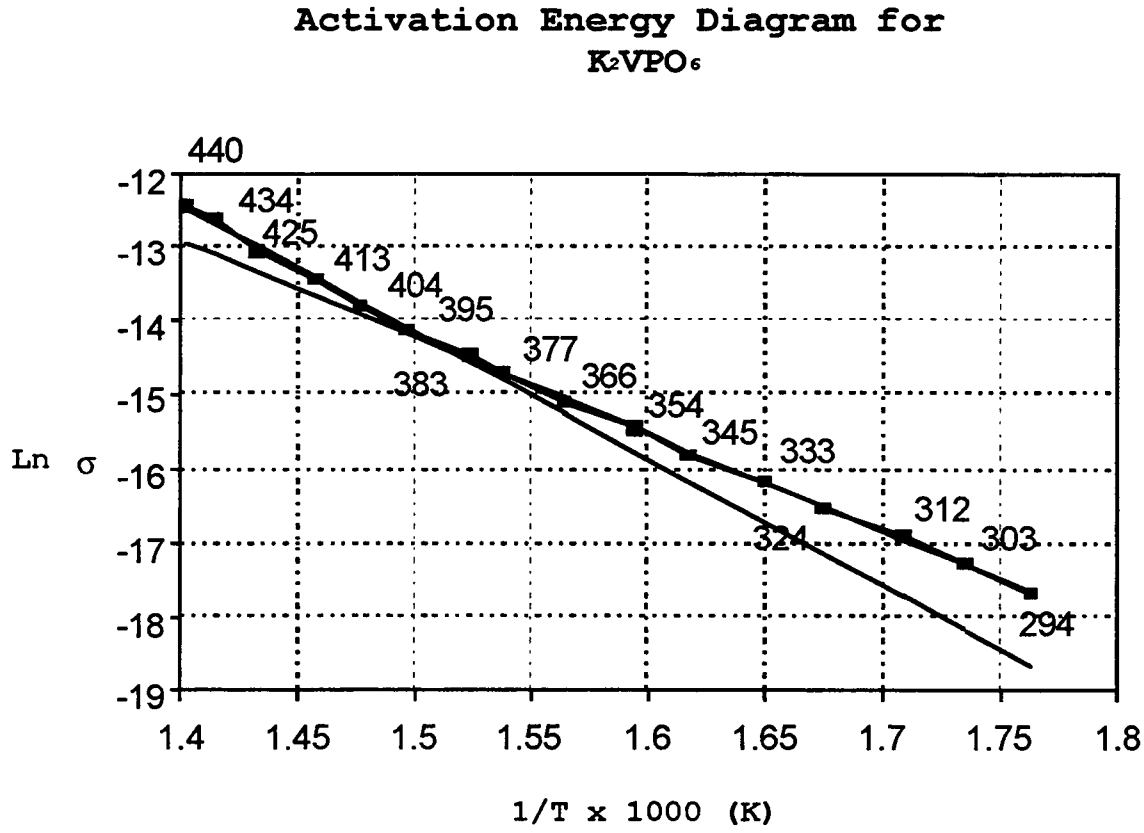

Figure 5.6 Ln σ versus 1/T for K_2VPO_6.

Table 5.5

Impedance Data for Li_2VPO_6

Temperature (°C)	Resistance (Ω)	Conductivity (Ω^{-1} cm^{-1})
451	572963	1.819×10^{-7}
440	773419	1.347×10^{-7}
430	1044007	9.981×10^{-8}
420	1452181	7.176×10^{-8}
408	1979940	5.263×10^{-8}
397	2809669	3.709×10^{-8}
387	3987110	2.613×10^{-8}
378	5657979	1.842×10^{-8}
369	8525543	1.222×10^{-8}
357	12466771	8.358×10^{-9}
348	18229967	5.716×10^{-9}
337	27195915	3.832×10^{-9}

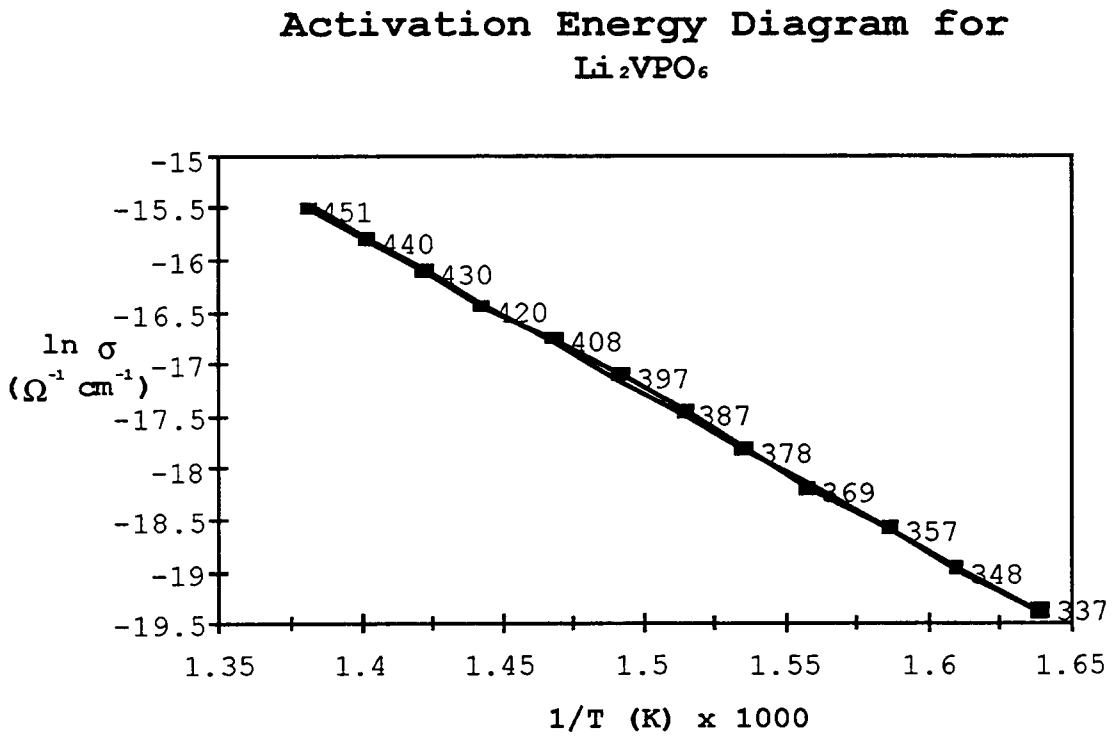

Figure 5.7 Ln σ versus 1/T for Li_2VPO_6.

5.4 Discussion

From the structures, it was hoped that these materials would be good candidates for ionic conduction. The criteria for good ionic conduction is to have loosely bound ions that may hop from one site to another. In order for this to be achieved, there should be channels for the ions to move through. From the structures, the criteria seemed to have been met since the structures could be described as either a layered material with ions in between the sheets (Li_2VPO_6) or as a stacked material with ions in the tunnels (Na_2VPO_6, K_2VPO_6). Attempts at making alkali cation vacancies has been attempted using molybdenum ($K_{2-x}V_{1-x}Mo_xPO_6$ and $Na_{2-x}V_{1-x}Mo_xPO_6$) and sulfur ($K_{2-x}VP_{1-x}S_xO_6$ and $Na_{2-x}VP_{1-x}S_xO_6$). This resulted in either a green glass phase in both cases or a binary phase of molybdenum phosphates and alkali vanadates and vanadium sulfates and alkali phosphates.

The impedance plots all showed well described semicircumferences at the high frequency end, whereas at the low frequency domains, straight lines with a slope close to 1 appeared. This observation is explained by a modification of the equivalent circuit by addition of a new element, the Warburg impedance (Z_w), which takes into

account a mixed mechanism of diffusion conduction plus ionic transport (6). This may be placed in series with the resistance R_b and in parallel with the capacitance C_b (7).

The activation energy diagrams shown for K_2VPO_6 and Na_2VPO_6 in Figures 5.5 and 5.6 show two different slopes. This is usually common in materials in which there is a phase transition and thus a different mechanism for ionic conductivity (8). There is no phase transition observed for K_2VPO_6 and Na_2VPO_6 up to their melting points. However, there are two different sites for the sodium and potassium ions. It may be that at the lower temperatures one ion is more free to move than the other and with increasing temperature the other ion has overcome its activation energy barrier to migrate. The Li_2VPO_6 compound shows well behaved Arrhenuis type behavior as shown in Figure 5.7. The activation energies for all these compounds is quite high when comparing to sodium β-Alumina which has an activation energy of 4.89 Kcal/Mole (4). If one compares to NaCl with an activation energy of 19 KCal/Mole (1), they are still rather high. The conductivity of these samples is also rather low compared to good ionic conductors. For example, sodium β-Alumina

at 350 °C has a conductivity of ~1.35 Ω^{-1} cm^{-1}. The conductivity at 350 °C for NaCl is roughly 6.4 x 10^{-8}. Comparing this to values in Tables 5.3 to 5.5, it can be seen that these compounds more closely resemble NaCl and are thus not good ionic conductors.

5.5 References

1. Anthony R. West, *Solids State Chemistry and its applications*, John Wiley and Sons (1984), Appendix A8

2. Anthony R. West, *Solid State Chemistry and its applications*, John Wiley and Sons (1984), Chapt. 13

3. I.M. Hodge, M.D. Ingram and A.R. West, *J. Electroanal. Chem.*, **74**, 125-143 (1976)

4. I.M. Hodge, M.D. Ingram and A.R. West, *Electroanal. Chem. an Interfacial Electrochem.*, **58**, 429-432, (1975)

5. R.D. Armstrong, T. Dickinson and P.M. Willis, *Electroanal. Chem. and Interfacial Electrochem.*, **53**, 389-405, (1974)

6. A.L. Oliveira, O. O. Damasceno, J. Oliveira, E.J.L. Schouler, *Mater. Res. Bull.*, **21**, 877 (1986)

7. Casal B., Ruiz-Hitzky E., Crespin M., Tinet D., Galvan J.C., *J. Chem. Soc., Faraday Trans.*, **85**, 4167, (1989)

8. N. El Horr, A. Hammou, M.Bagieu, *J. Solid State Chem.*, **90**, 361-366 (1991)

6. THERMAL EXPANSION BEHAVIOR OF A SOLID SOLUTION OF ZrV_2O_7 AND ZrP_2O_7

6.1 Introduction

The compound ZrV_2O_7, first discovered by Peyronel (1), has been shown to undergo a very rapid thermal expansion from room temperature up to 120 °C, after which the thermal expansion becomes negative up to the decomposition temperature of 800 °C (2).

Negative thermal expansion is not new in that some materials have shown a net volume decrease as the temperature is increased. However, most materials showing very low or negative thermal expansion are actually composed of crystallites which show very anisotropic thermal expansion. Contraction in one dimension is typically coupled with the expansion in the other two dimensions. This phenomena is evident in $NaZr_2(PO_4)_3$ (3,4,5,6,7) (NZP), $(ZrO)_2P_2O_7$ (8), and β-eucryptite (9).

Only the ZrP_2O_7 type structure appears to have the capacity for isotropic negative thermal expansion over an extended temperature range (10). A family of $A^{4+}M_2^{5+}O_7$ compounds exist with the cubic structure shown in Figure 6.1, which may be described by its relationship to the

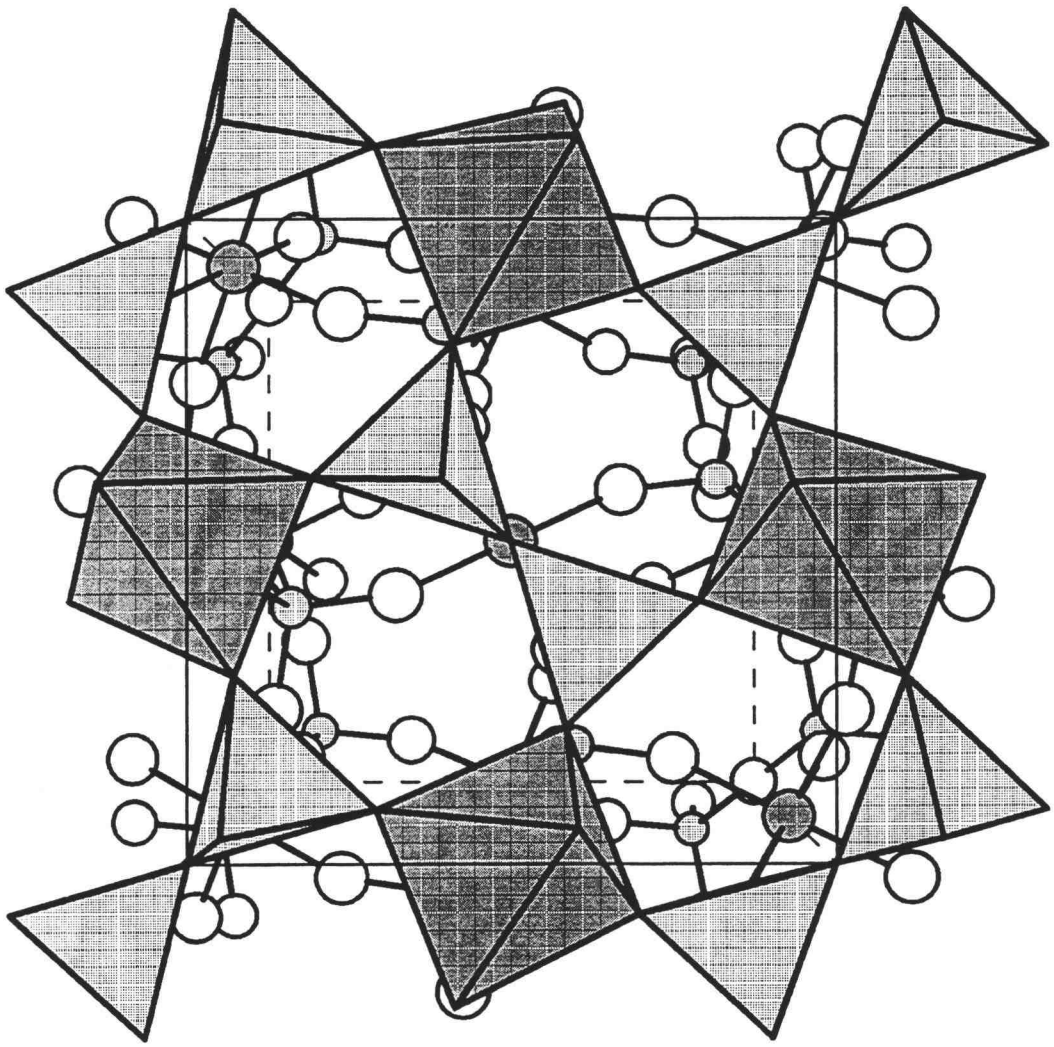

Figure 6.1 Structure of $A^{4+}M_2^{5+}O_7$ type compounds. Shaded octahedra and large shaded circles are A^{4+}, shaded tetrahedra and small shaded circles are M^{5+}. Large open circles represent oxygen.

NaCl structure. In this description the cation is A^{4+} and the anion is $(M_2O_7)^{4-}$. The ordered orientation of the $(M_2O_7)^{4-}$ group necessarily lowers the symmetry of the NaCl structure. The space group for NaCl is Fm3m while the highest symmetry space group possible for this type of material is Pa3. The A^{4+} cation may be Th, U, Pu, Ce, Hf, Zr, Ti, Mo, Re, W, Pb, Sn , Ge, or Si when M is phosphorous (11,12,,13,14,15,16,17,18,19,20,21,22,23,24). Double substitution on to the A^{4+} site is possible leading to a family of the type $A^{3+}_{0.5}A^{5+}_{0.5}P_2O_7$ where A^{3+} may be Bi, Sb or a rare earth and A^{5+} may be Nb, Ta or Sb (25). One form of $Sb^{3+}Sb^{5+}(P_2O_7)_2$ has a structure very closely related to that of ZrP_2O_7 (26). Tantalum and niobium phosphates are also known to have this basic structure type (27). Their exact composition and structure is uncertain, but the appropriate formulation might be $Nb_{0.8}P_2O_7$. Arsenates can also have the cubic ZrP_2O_7 structure when A^{4+} is Zr or Th (28,29). The only vanadates known to have this structure are HfV_2O_7 and ZrV_2O_7 (30,31).

At high temperatures, these $A^{4+}M^{5+}_2O_7$compounds presumably have the ideal structure of Figure 6.1. However, apparently all of these compounds possess phase

transitions well above room temperature. Below the phase transition, these compounds appear to retain their cubic symmetry but a superstructure appears, requiring a tripling of the unit cell edges. The thermal expansion of $A^{4+}M_2^{5+}O_7$ phases might be considered normal up to the phase transition. However, above the phase transition the thermal expansion can be extremely low and even become negative. In the case of ZrV_2O_7 and HfV_2O_7 the thermal expansion is highly negative above 150 °C to their decomposition temperature of about 800 °C.

In the system investigated here, the material has been examined by powder x-ray diffraction (both room temperature and high temperature), high resolution powder neutron diffraction (room temperature and high temperature), dilatometry, and computer simulations using distance least squares. All evidence seems to point to a cubic space group which leads to a new type of material with an isotropic negative thermal expansion behavior.

Nuclear magnetic resonance (NMR) was also used to support the formation of a superstructure for ZrP_2O_7 and ZrV_2O_7 (32). It was also used to probe the solid solution to observe if the vanadium and phosphorous would mix to form V-O-P groups or if the solid solution could be

described as a mixture of V-O-V and P-O-P groups randomly scattered throughout the sample. Also FTIR measurements were made to observe bending and stretching modes available to this material.

6.2 Experimental

It was found that large (i.e. > 0.05 cm) crystals of ZrV_2O_7 could not be formed in our lab. The difficulty lies in the fact that ZrV_2O_7 melts incongruently. Many different synthetic methods were tried such as with PbO, B_2O_3, and alkali salt fluxes, but these were unsuccessful due to the formation of vanadate compounds forming with the fluxes. It was observed that small crystals of ZrV_2O_7 formed on the bottom and sides of platinum crucibles. It was hoped that large crystals could be formed in a melt rich in V_2O_5 and then raised out of the melt with a platinum mesh screen. The platinum mesh screen was placed in the bottom of the platinum crucible and a melt rich in V_2O_5 was allowed to slowly cool from 850 °C to 750 °C at a rate of 2 °C per hour. Then the screen was slowly taken out of the melt and left to hang over the melt for 24 hours. The furnace was then allowed to cool to room

temperature at a rate of 10 °C per hour. The mesh screen still had V_2O_5 on it and there were no large single crystals of ZrV_2O_7 seen under a microscope. Most crystals that were bigger than 0.05 cm showed cracking and dark material trapped inside.

To make polycrystalline ZrV_2O_7 it was found that a solution method of mixing the components worked the best compared to solid state reactions of the oxides. First, a solution of $ZrOCl_2 \bullet 8\ H_2O$ (reagent, Teledyne Wah Chang Albany) was made by dissolving 28.9695 g (0.0898 mol) $ZrOCl_2 \bullet 8\ H_2O$ in 150 ml of H_2O. A second solution is made by dissolving 21.0316 g (0.1797 mol) NH_4VO_3 (99%, Johnson Matthey) in 150 ml H_2O. To the NH_4VO_3 solution, concentrated HNO_3 is added to keep the pH to about 2 while constant stirring and heating is applied. The $ZrOCl_2$ solution is added to the NH_4VO_3 solution while being heated and stirred. The solution turns to a yellow/red gel. This in then placed in a drying oven at 120 °C overnight until all the water is evaporated. The solid that remains is then ground in an agate mortar and placed into an alumina crucible and heated in air for 24 hours at 750 °C. The same method is applied in making ZrP_2O_7,

using $(NH_4)_2HPO_4$ (reagent, mallinkrodt), but the final firing temperature is raised to 900 °C. The solid solution series was made by combining the stoichiometric amounts of $(NH_4)_2HPO_4$ and NH_4VO_3 in solution and adding the $ZrOCl_2 \bullet 8\ H_2O$ to the solution. The final firing temperature being 750 °C.

Experiments were performed to try to insert lithium into the material. This was performed by reacting polycrystalline ZrV_2O_7 with n-butyl lithium in hexane (dried previously with CaH_2) to form $Li_xZrV_2O_7$ as shown below.

$$ZrV_2O_7 + xC_4H_9Li \rightarrow Li_xZrV_2O_7 + x/2\ C_8H_{18}$$

The material changed from a brown yellow color to black upon addition of n-butyl lithium indicating a reduction of the vanadium. Powder x-ray diffraction showed no evidence of change in the unit cell size, suggesting that the lithium reacted only with the surface of the polycrystalline material. If excess n-butyl lithium was used (i.e. $x > 1$), the material became amorphous. When the sample was heated to 250 °C, x-ray diffraction showed $LiV_3O_{7.9}$ as the major phase.

Attempts at substituting Sn and Ti on the Zr site resulted in mixed phase materials. Partial subsitution on the Zr site had also failed for compositions that contained vanadium and phosphorous (i.e. $ZrV_{2-x}P_xO_7$ $x < 2$).

Thermal expansion measurements were done on a Netzsh STA 401 thermal analysis system dilatometer. The sample holder was constructed from quartz and a software calibration routine was used for dilatometer corrections as explained in Appendix I. The pellets used were made from a die constructed to make pellets 25 cm long by 1.5 cm wide. All pellets were annealed at 750 °C for approximately 4 hours before being used on the dilatometer.

X-ray diffraction experiments were done on a Siemens D5000 powder diffractometer. A hot stage constructed for high temperature powder X-ray diffraction experiments and aluminum powder was used as an internal standard (α = 22 x 10^{-6} $°C^{-1}$). The temperature was determined from a type K thermocouple placed in the sample, and the aluminum peaks were used as reference points to account for the sample height variation at different temperatures. The corrected peak positions were used to refine the unit cells of the samples using the software from Siemens.

Rietveld refinements were carried out on X-ray and neutron powder diffraction data. Neutron diffraction data were collected using the beam line at Brookhaven National Laboratories. The data were refined using Rietan, GSAS and Profil Rietveld programs. Due to the tripling of the unit cell, which leads to a superstructure with a volume 27 times larger than the subcell, a computer modeling program called distance least squares, DLS (33), was used to help in the unraveling of the atomic positions by using predicted distances as observations in a least squares refinement. A bug was found in the Rietan program which did not account for h0l peaks when l < h. This bug was subsequently fixed and the program was modified to refine up to 250 independent variables for the refinement of the superstructure.

6.3 Results

The synthesis of the $ZrV_{2-x}P_xO_7$ powders prepared from aqueous solutions showed a gradual change in the cubic cell lattice constants. The cell edges versus composition can be seen in Figure 6.2. From this, one can observe that a solid solution between ZrP_2O_7 and ZrV_2O_7 forms a

material whose lattice constant reflects the composition of the material very well. The value of a in Figure 6.2 ignores the 3 x 3 x 3 superstructure when it is present. The solid solution members show this tripling behavior only towards the very ends of the series.

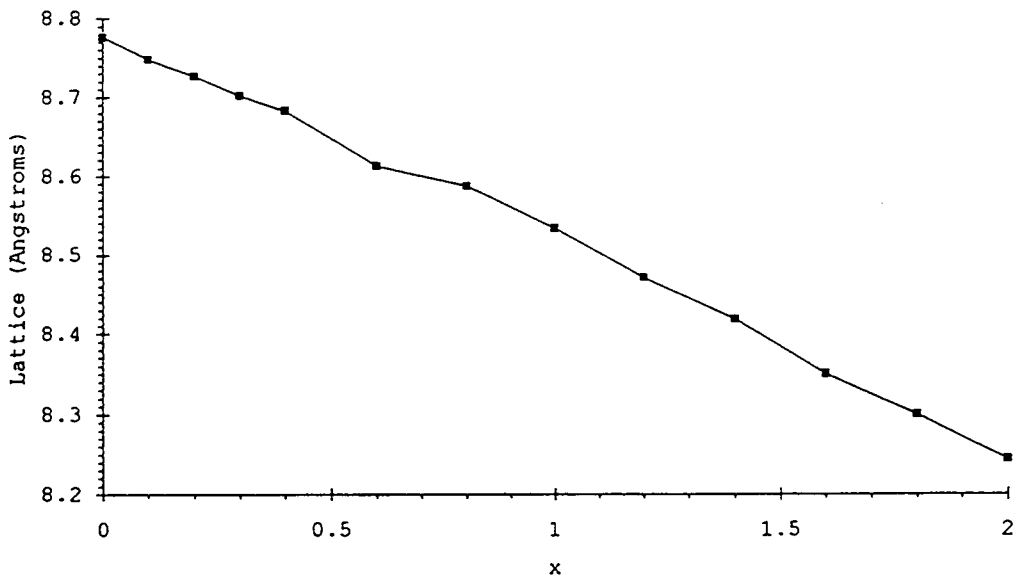

Figure 6.2 Lattice Constant Versus Composition for $ZrV_{2-x}P_xO_7$, using refined powder x-ray diffraction data.

A dilatometer was used to collect thermal expansion data for the $ZrV_{2-x}P_xO_7$ series. This is shown in Figures 6.3 and 6.4. A list of the coefficients of thermal expansion is shown in Table 6.1. One can notice in Figure 6.3 that the end members of the solid solution series show pronounced thermal expansion just above room temperature.

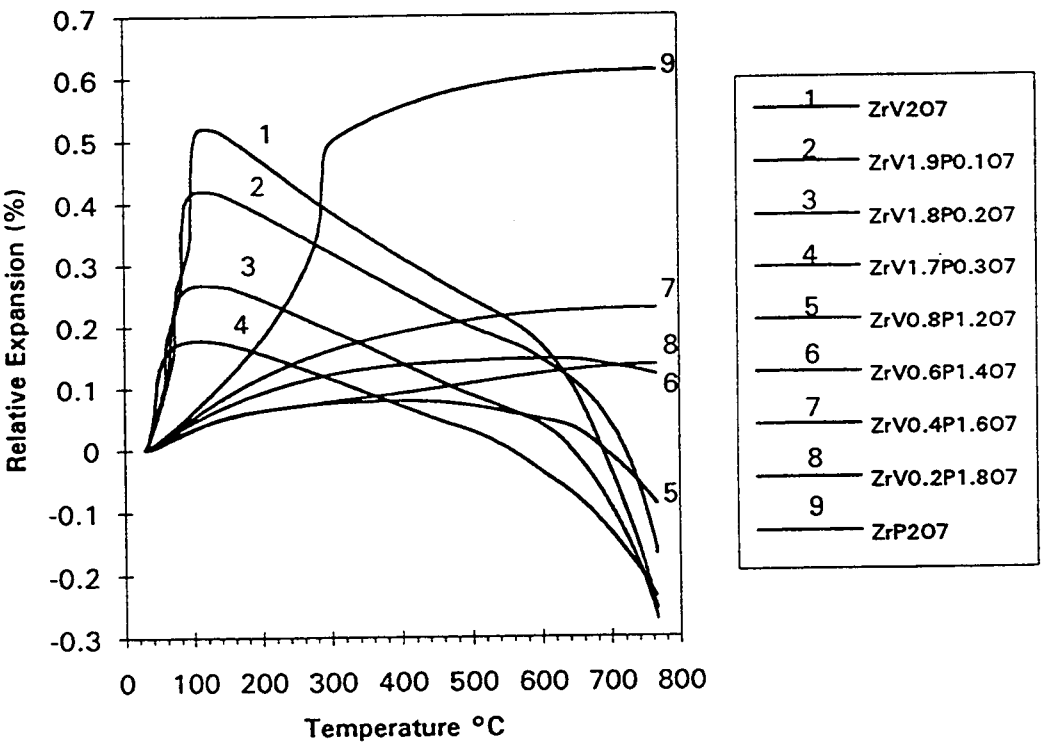

Figure 6.3 Linear thermal expansion versus temperature for $ZrV_{2-x}P_xO_7$ using dilatometer data.

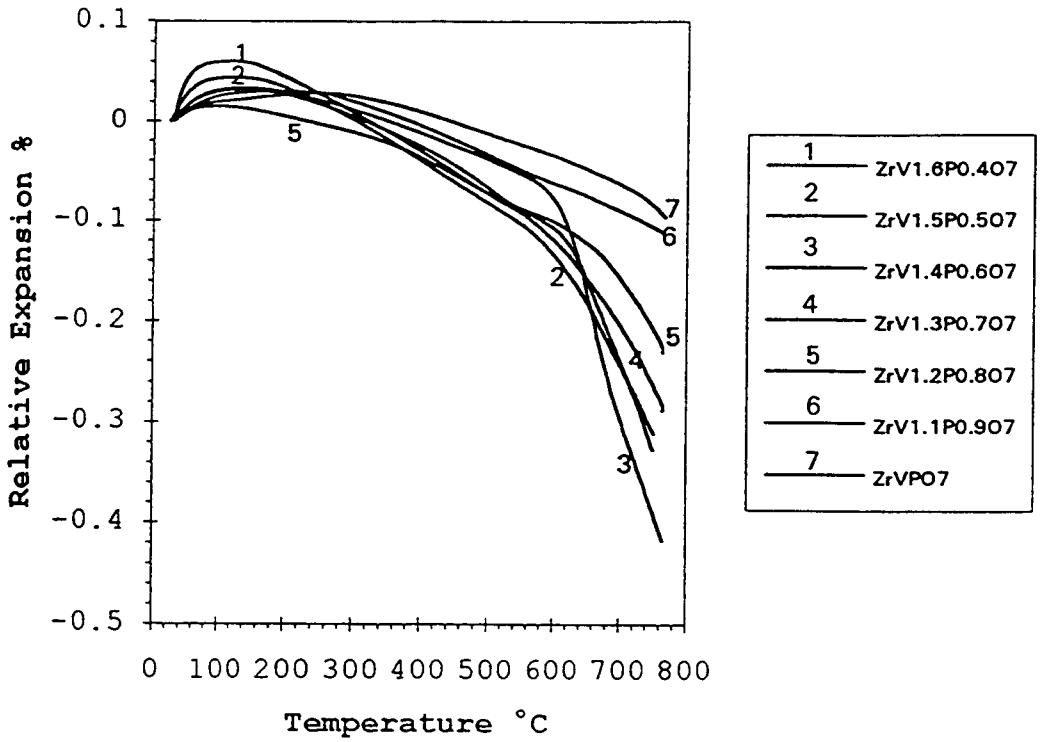

Figure 6.4 Linear thermal expansion versus temperature for $ZrV_{2-x}P_xO_7$ using dilatometer data.

In fact the ZrP_2O_7 and ZrV_2O_7 end members show very large thermal expansion behavior up to the phase transitions, after which the thermal expansion diminishes considerably or becomes negative. From the behavior of the end members, one would not predict the behavior of the series as shown in Figure 6.4.

Table 6.1

Coefficients of Linear Thermal Expansion
$\alpha = X \times 10^{-6}\ ^{\circ}C^{-1}$

ZrV_2O_7	α = 37.9 (30-70 °C)	α = 38.6 (75-95 °C)	
	α = -7.4 (120-601 °C)	α = -25.2 (649-786 °C)	
$ZrV_{1.9}P_{0.1}O_7$	α = 39.3 (30-55 °C)	α = 40.8 (65-81 °C)	
	α = -5.9 (126-602 °C)	α = -18.7 (602-787 °C)	
$ZrV_{1.8}P0._2O_7$	α = 34.4 (30-109 °C)	α = -5.1 (130-624 °C)	
	α = -20.1 (621-767 °C)		
$ZrV_{1.7}P_{0.3}O_7$	α = 25.8 (30-101 °C)	α = -4.4 (101-600 °C)	
	α = -11.8 (600-765 °C)		
$ZrV_{1.6}P_{0.4}O_7$	α = 10.5 (30-91 °C)	α = -5.3 (121-762 °C)	
$ZrV_{1.5}P_{0.5}O_7$	α = 5.8 (25-110 °C)	α = -3.7 (110-600 °C)	
	α = -11.7 (600-765 °C)		
$ZrV_{1.4}P_{0.6}O_7$	α = 5.2 (30-100 °C)	α = -2.5 (124-600 °C)	
	α = -20.2 (600-765 °C)		
$ZrV_{1.3}P_{0.7}O_7$	α = 4.4 (25-110 °C)	α = -2.9 (110-600 °C)	
	α = -14.9 (600-766 °C)		
$ZrV_{1.2}P_{0.8}O_7$	α = 4.3 (30-76 °C)	α = -2.3 (76-601 °C)	
	α = -7.3 (601-766 °C)		
$ZrVPO_7$	α = 3.8 (30-95 °C)	α = -0.2 (96-245 °C)	
	α = -2.3 (243-768 °C)		
$ZrV_{0.8}P_{1.2}O_7$	α = 2.1 (30-395 °C)	α = -1.6 (394-640 °C)	
	α = -9.5 (640-766 °C)		
$ZrV_{0.6}P_{1.4}O_7$	α = 2.5 (30-604 °C)		

Table 6.1 (Continued)

$ZrV_{0.4}P_{1.6}O_7$	α = 3.9 (30-603 °C)	
$ZrV_{0.2}P_{1.8}O_7$	α = 4.5 (30-748 °C)	
ZrP_2O_7	α = 12.8 (30-270 °C)	α = 2.62 (300-769 °C)

The X-ray data of ZrV_2O_7 was taken as a function of temperature and is shown in Figure 6.5. The limit of the hot stage temperature did not allow the ZrP_2O_7 phase transition to be observed using powder x-ray diffraction. As one can see, the shape of the curve in Figure 6.5 matches well with the dilatometry results shown in Figure 6.3. From the data shown in Table 6.2 one can calculate the thermal expansion coefficients as 39 x 10^{-6} °C $^{-1}$ at 20 to 70 °C, and -6.8 x 10^{-6} °C $^{-1}$ at 120 to 240 °C.

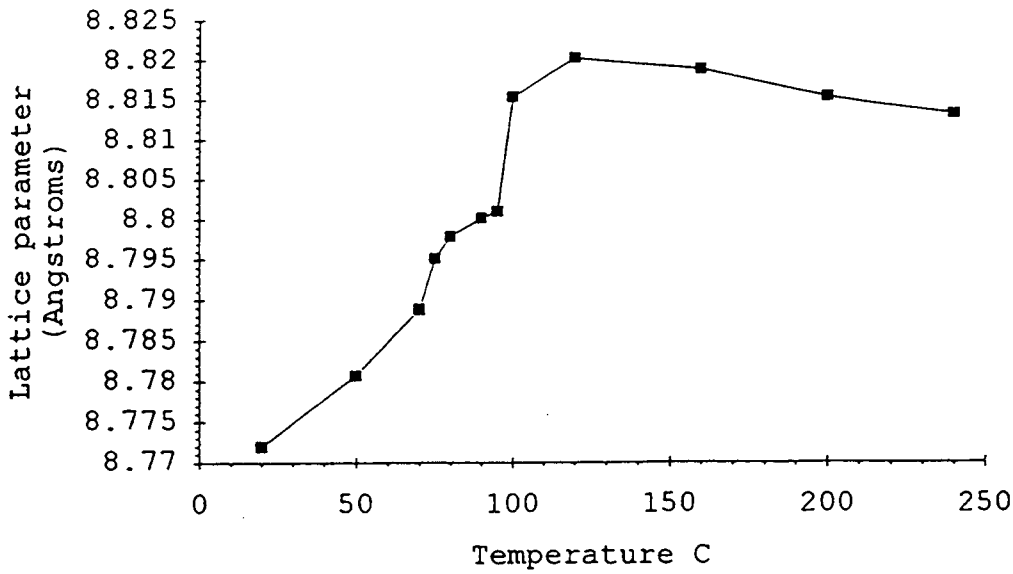

Figure 6.5 Lattice constant versus temperature for ZrV_2O_7 using high temperature X-ray Data.

These values match those of Table 6.1 very well. In the vicinity of the phase transitions, two cubic phases of ZrV_2O_7 frequently were observed by x-ray diffraction shown in Figures 6.6 and 6.7. This could be due to a thermal gradient in the sample. However, these phase transitions are first order; therefore, it is possible that the two phases coexisted at the same temperature due to a kinetic barrier to transformation.

Table 6.2

Lattice Constant of ZrV_2O_7 at various Temperatures

Temperature	Lattice (Å)
20 °C	8.772(1)
50 °C	8.7807(5)
70 °C	8.7889(6)
71 °C	8.7953(6)
75 °C	8.7953(4)
80 °C	8.7980(6)
90 °C	8.8003(5)
95 °C	8.8011(3)
98 °C	8.8038(7)
99 °C	8.8154(8)
100 °C	8.8154(9)
120 °C	8.8202(5)
160 °C	8.8187(5)
200 °C	8.8154(6)
240 °C	8.8130(5)

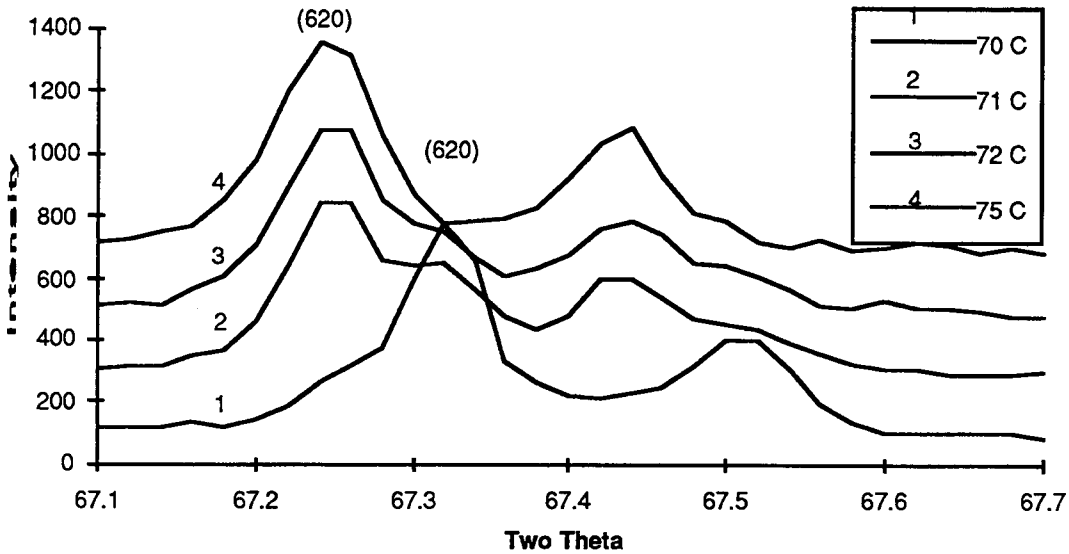

Figure 6.6 High temperature powder X-Ray diffraction of ZrV_2O_7 showing the first phase transition.

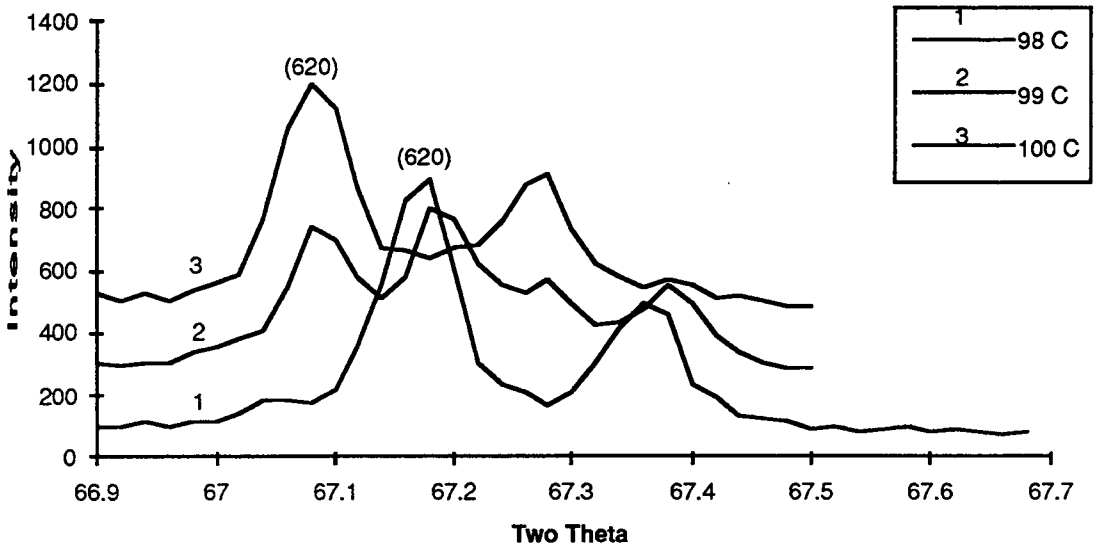

Figure 6.7 High temperature powder X-ray diffraction of ZrV_2O_7 at the second phase transition.

DSC measurements starting at -80 °C up to 200 °C was performed on ZrV_2O_7 and showed sharp transitions at 77 °C and 102 °C corresponding to the abrupt increase in volumes shown in Figures 6.3 and 6.5. The sharpness of these transitions and the hysteresis of these transitions indicates that they are first order. The 3 x 3 x 3 superstructure is observed above the first transition, but no superstructure was observed above the second transition. An attempt was made to follow both of these transitions in a $ZrV_{2-x}P_xO_7$ series. For x = 0.01, the

two transitions dropped to 68 °C and 89 °C; for x = 0.2, the two transitions had dropped again to 48 °C and 67 °C. As x further increased, the transitions became more diffuse as indicated by a broadening and weakening of the DSC peaks. For x = 0.3, only one peak at about 53 °C was apparent. No DSC peaks were ever found below room temperature.

A description of the atomic displacemments involved in the formation of the 3 x 3 x 3 superstructure is challenging. From the four atoms in the subcell shown in Table 6.3 one generates 50 atom positions for the

Table 6.3

Subcell Atomic Positions for $A^{4+}M_2^{5+}O_7$

Atom	Position	X	Y	Z
A	(4a)	0.0	0.0	0.0
M	(8c)	0.3833	0.3833	0.3833
O1	(4b)	0.5	0.5	0.5
O2	(24d)	0.441	0.202	0.408

Table 6.4

Supercell Atomic Position Generated from Subcell

ATOM	POSITION	X	Y	Z	Translations From subcell*
A1	(24d)	0.3333	0.0	0.0	100,010,001
					200,020,002
A2	(24d)	0.3333	0.3333	0.0	110,011,101
					220,022,202
A3	(24d)	0.0	0.3333	0.6667	012,201,120
					021,102,210
A4	(24d)	0.3333	0.6667	0.3333	121,211,112
					221,122,212
A5	(8c)	0.3333	0.3333	0.3333	111,222
A6	(4a)	0.0	0.0	0.0	000
M1	(24d)	0.4610	0.1277	0.1277	100,010,001
M2	(24d)	0.4610	0.4610	0.1277	110,011,101
M3	(24d)	0.7943	0.1277	0.1277	200,020,002
M4	(24d)	0.7943	0.7943	0.1277	220,022,202
M5	(24d)	0.1277	0.4610	0.7943	012,201,120
M6	(24d)	0.1277	0.7943	0.4610	021,102,210
M7	(24d)	0.4610	0.7943	0.4610	121,112,211
M8	(24d)	0.4610	0.7943	0.7943	122,212,221
M9	(8c)	0.7943	0.7943	0.7943	222
M10	(8c)	0.4610	0.4610	0.4610	111
M11	(8c)	0.1277	0.1277	0.1277	000
O1**	(24d)	0.5	0.1667	0.1667	100,010,001
					122,212,221
O2**	(24d)	0.8333	0.1667	0.1667	200,020,002
					220,022,202
O3**	(24d)	0.5	0.5	0.1667	110,011,101
					112,211,121
O4**	(24d)	0.1667	0.5	0.8333	012,201,120
					210,021,102
O5**	(8c)	0.1667	0.1667	0.1667	000,222

Table 6.4 (Continued)

O6**	(4b)	0.5	0.5	0.5	111
O7	(24d)	0.1470	0.0670	0.1360	000
O8	(24d)	0.4800	0.0670	0.1360	100
O9	(24d)	0.1470	0.4010	0.1360	010
O10	(24d)	0.1470	0.0670	0.4690	001
O11	(24d)	0.4800	0.4010	0.1360	110
O12	(24d)	0.4800	0.6700	0.4690	101
O13	(24d)	0.1470	0.4010	0.4690	011
O14	(24d)	0.4800	0.4010	0.4690	111
O15	(24d)	0.8140	0.0670	0.1360	200
O16	(24d)	0.1470	0.7340	0.1360	020
O17	(24d)	0.1470	0.0670	0.8030	002
O18	(24d)	0.8140	0.7340	0.1360	220
O19	(24d)	0.8140	0.0670	0.8030	202
O20	(24d)	0.1470	0.7340	0.8030	022
O21	(24d)	0.8140	0.7340	0.8030	222
O22	(24d)	0.1470	0.4010	0.8030	012
O23	(24d)	0.1470	0.7340	0.4690	021
O24	(24d)	0.4800	0.7340	0.1360	120
O25	(24d)	0.4800	0.7340	0.4690	121
O26	(24d)	0.4800	0.4010	0.8030	112
O27	(24d)	0.4800	0.7340	0.8030	122
O28	(24d)	0.4800	0.0670	0.8030	102
O29	(24d)	0.8140	0.0670	0.4690	201
O30	(24d)	0.8140	0.4010	0.1360	210
O31	(24d)	0.8140	0.4010	0.4690	211
O32	(24d)	0.8140	0.4010	0.8030	212
O33	(24d)	0.8140	0.7340	0.4690	221

*Generators for supercell used in the formula (xsub+translation)/3, (ysub+translation)/3, (zsub+translation)/3.

** Generated from O1 of the subcell.

supercell shown in Table 6.4. This corresponds to refinement of 4 positional parameters of the subcell to refinement of 134 positional parameters of the supercell. Indeed the refinement of the superstructure becomes increasingly difficult when one adds thermal parameters, scale factor, peak shape parameters, to the list of powder refinement variables. Our approach was similar to that used in refining the superstructure for SiP_2O_7. Least-squares refinements were carried out from various different starting models calculated from DLS, and distance constraints were employed in the refinement. Also, the thermal parameters for oxygen atoms on the three fold axes were refined anisotropically to simulate the likely disordered bending of the M-O-M bond involving these oxygens.

The proposed 3 x 3 x 3 superstructure is supported by NMR measurements. Room temperature high resolution phosphorous NMR of ZrP_2O_7 was least squares fit to 11 Lorentzian peaks and 1 Gaussian peak. Eight of the Lorentzian peaks were constrained to unit intensity, and three were constrained to one third unit intensity. The three peaks with one third unit intensity account for 11.1% of the intensity of the Lorentzian peaks. The model

fit the data reasonably well and is consistent with the 3 x 3 x 3 superstructure. The Gaussian peak is assumed to be the result of an unknown impurity phase representing 4.4% of the total intensity.

NMR (^{31}P) was used to identify the V-O-P and V-O-V bonding configurations. The ratio of the number of V-O-P to P-O-P bonds was measured to be 0.28 and 4.37 for $ZrV_{0.4}P_{1.6}O_7$ and $ZrVPO_7$ respectively. No P-O-P bonds were observed in the $ZrV_{1.7}P_{0.3}O_7$ material. If sites were occupied randomly these ratios would be 0.40 and 2.0 respectively. Therefore, a mixture of P_2O_7 and V_2O_7 groups is favored over PVO_7 groups for $ZrV_{0.4}P_{1.6}O_7$, and VPO_7 groups are favored for $ZrVPO_7$. In the mixed materials, no superstructure is observed in the NMR spectra. Also the two distinct sites for V_2O_7 and PVO_7 groups were not resolved in the vanadium spectra. In the ^{51}V spectra of ZrV_2O_7, evidence for the 3 x 3 x 3 superstructure remains at 80 °C, but this structure is washed out in the 90 °C spectrum, consistent with a phase transition in this temperature range. Also room temperature IR spectra along with empirical band assignments (34,35,36,37) were obtained for the ZrV_2O_7, $ZrVPO_7$ and ZrP_2O_7 compositions shown in Figure 6.8. Many

of the peaks have shifted in the mixed material and other bending modes have appeared.

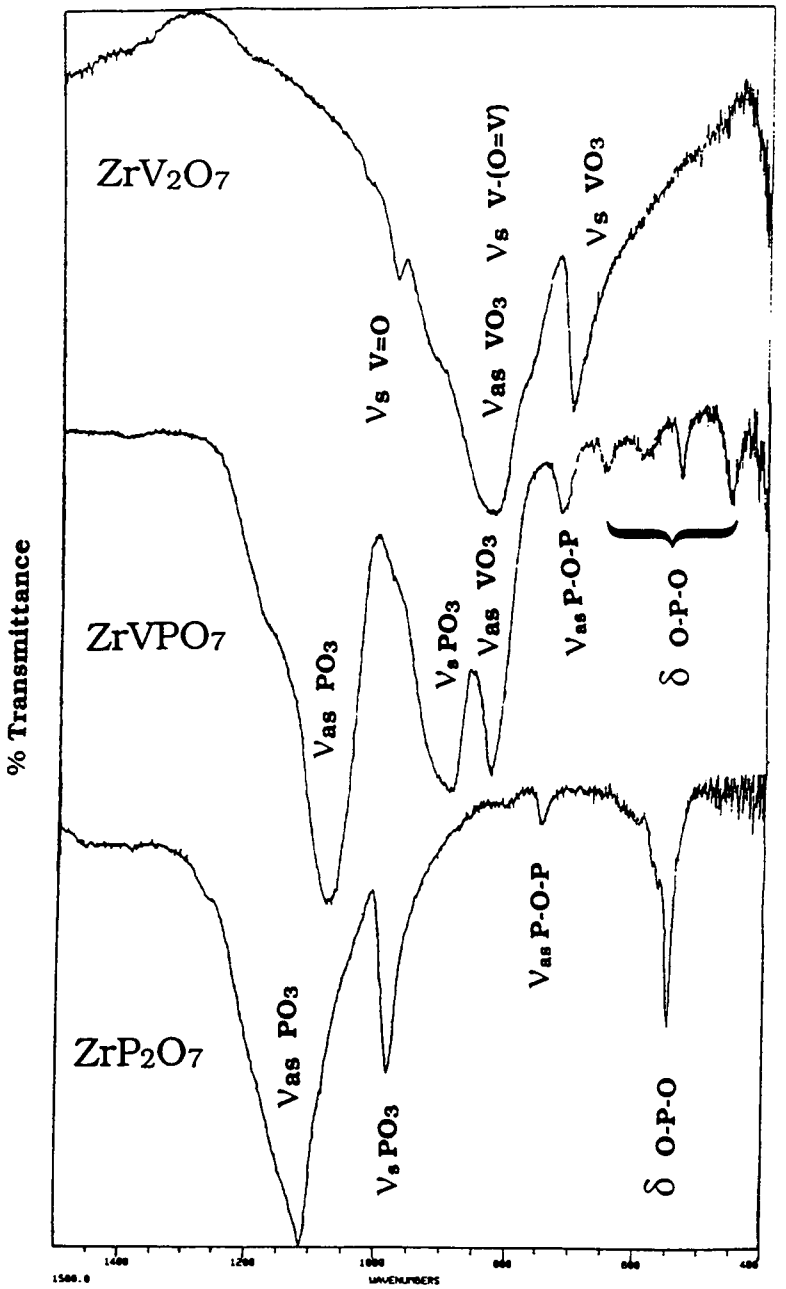

Figure 6.8 IR spectra of ZrV_2O_7, $ZrVPO_7$ and ZrP_2O_7.

6.4 Discussion

Contraction, rather than expansion, with increasing temperature can apparently be caused by different structural features for different materials. In most casis of negative volume expansion, the normal positive thermal expansion of chemical bonds in some directions actually causes lattice contraction in other directions. Such materials are then highly anisotropic in their thermal expansion properties. The net effect can be a very low volume thermal expansion which can be slightly negative. An alternative explanation must be sought for isotropic compounds showing negative thermal expansion.

The thermal expansion behavior of the end members of the $ZrV_{2-x}P_xO_7$ series show normal behavior until close to the phase transition temperatures. Polyhedra twisting probably occurs during the abrupt increases in volume. The unusual negative thermal expansion may be explained as being due to bending mode vibrations of the network. It is well known that the average O-O distance in CO_2 decreases with increasing temperature due to the bending mode in this molecule. Likewise, an M-O-M unit is susceptible to an decrease in the M-M distance with

increasing temperature under certain conditions. Most important is that the M-O bond be highly covalent. This has two intimately related consequences. One is that the thermal expansion of the M-O bond will be very small; the other is that thermal motion of oxygen will be very small along the direction of the M-O bonds. The thermal motion of oxygen perpendicular to M-O-M must be relatively high, and this normally occurs. A special case exists where the lattice symmetry requires that the M-O-M bond angle be 180°. Such an angle is generally not favorable, and this 180° instability is usually attributed to the cost of sp hybridization for oxygen. A description of the 180° M-O-M linkage situation is shown with the potential wells in Figure 6.9. The well is sharply defined for interactions along the M-O-M linkage, but is very broad for interactions perpendicular to the linkage. The bump in the middle of the broad maximum is attributed to the instability of the 180° bond angle of the M-O-M linkage. A consequence of the broad potential well is that M-O-M bond angle is likely to deviate strongly from 180° at high temperatures at any instant of time. However, the average M-O-M angle is 180°. With increasing temperature, maintaining the appropriate M-O distance

causes the M-M distance to decrease. If the M-O-M linkage only occurs in one direction, negative thermal expansion might be expected only in that direction. In the case of the $A^{4+}M^{5+}{}_2O_7$ family, the M-O-M linkage occurs in all three dimensions due to the cubic symmetry. The negative thermal expansion is therefore isotropic.

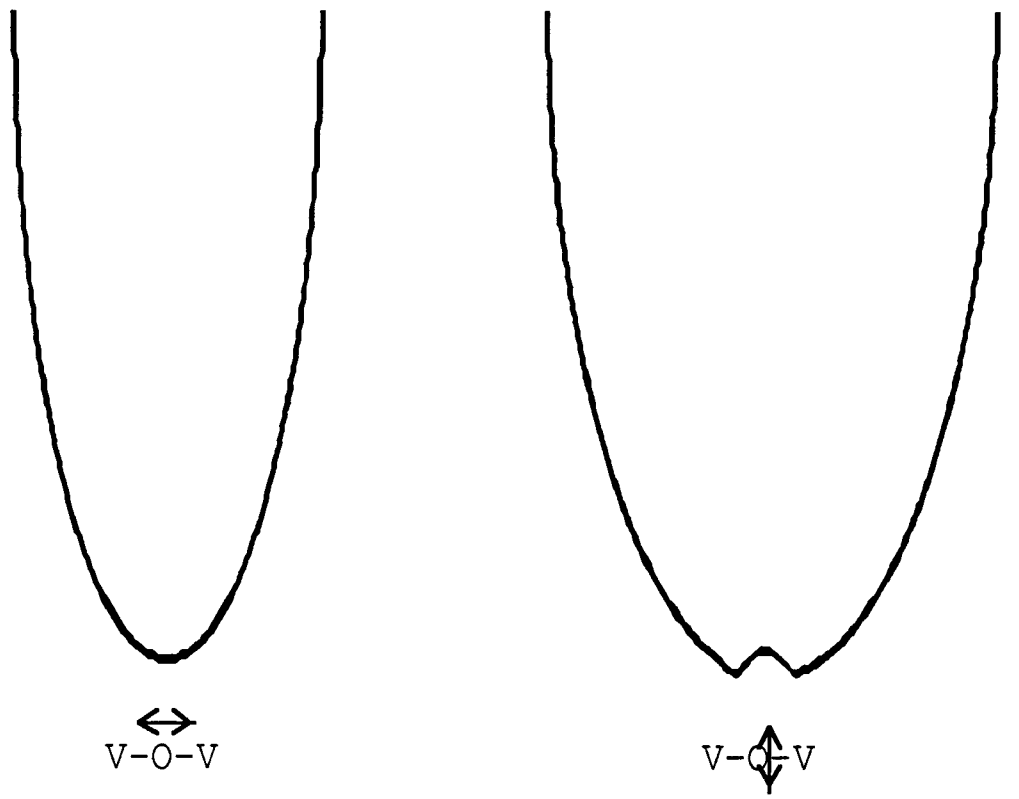

Figure 6.9 Potential Wells for O in M-O-M.

As the temperature is decreased, a common phenomenon is a phase transition to lower symmetry where the M-O-M angle is no longer required to be 180°. In other words, the vibrating oxygen becomes trapped on one side of the maximum in Figure 6.9. The thermal expansion below this phase transition becomes normal in that the thermal expansion is due to bond expansion along the direction of the bond. The situation with respect to the instability of the 180° M-O-M linkages commonly occurs in other structures such as the perovskite structure. The M-O-M angles in AMO_3 perovskites are ideally 180°. Many perovskites have this high cubic symmetry at high temperatures, but a lattice distortion occurs as temperature decreases. The instability of the 180° M-O-M bond angle causes the MO_6 octahedra to tilt during these distortions. In the common orthorhombic distortion of the perovskite structure, all M-O-M angles have bent away from 180°, and this results in an increase in the primitive unit cell from one to four formula units.

The connectivity present in the cubic $A^{4+}M^{5+}{}_2O_7$ structure frustrates distortions which would eliminate the 180° M-O-M angles. Thus, negative thermal expansion

persists to lower temperatures than would occur without this frustration. Figure 6.10 shows the space groups which could occur as symmetry elements are removed from the ideal $A^{4+}M^{5+}{}_2O_7$ structure in space group Pa3. The transition which apparently always occurs is the one where the cubic cell edges are tripled but the space group remains Pa3. The primitive unit cell has increased from 4 to 108 formula units. Many of the three fold axes and inversion centers are lost in this transition, but some remain. This transition leads to eleven crystallographically distinct sites for tetrahedral M cations. Three of these remain on three fold axes which accounts for 11.1% of all such cations. In the ideal structure, all oxygen atoms of the M-O-M linkage were at inversion centers on the three fold axes. In the tripled cell, most of the M-O-M angles (89%) are free to bend away from 180°. However, one oxygen site remains on the three fold axis with an inversion center. The M-O-M

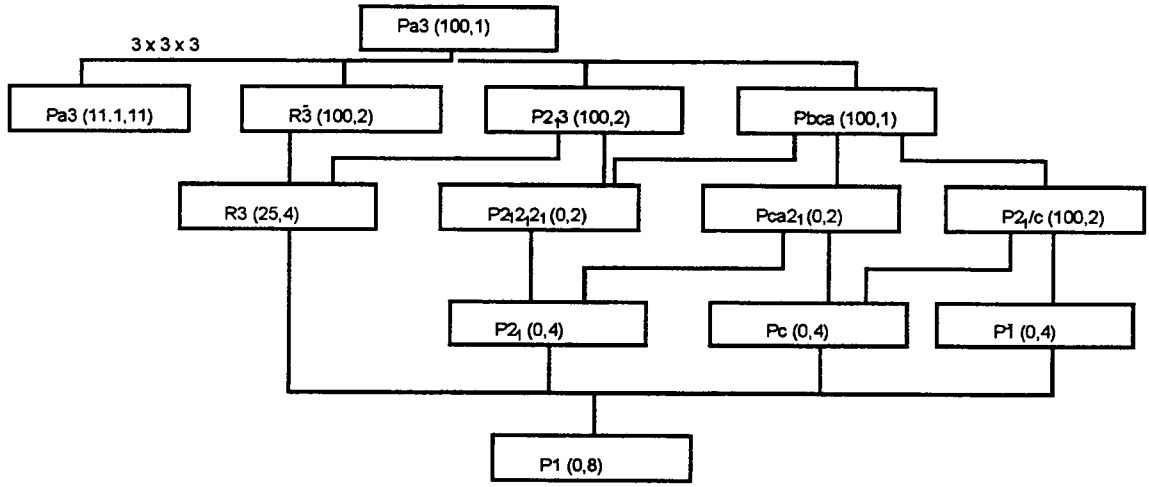

(%M-O-M 180°, # unique M)

Figure 6.10 Possible Space groups for $A^{4+}M^{5+}{}_2O_7$

angles involving these oxygen atoms are required by the space group symmetry to be 180°. However, this is only an average angle as indicated by the large thermal ellipsoids refined for these oxygen atoms. The cubic structure apparently always partially relieves the 180° M-O-M angle problem by adopting the cubic 3 x 3 x 3 superstructure. This occurs despite the fact that distortions to orthorhombic $P2_12_12_1$ or $Pca2_1$ would relieve all the 180° M-O-M angles without an increase in the primitive unit cell, and the number of crystallographic M atoms increase only to two as shown in Figure 6.10. Once the cubic 3 x 3 x 3 superstructure has formed, it becomes very difficult

to remove the remaining 180° M-O-M instabilities as shown in Figure 6.11. Distortion to orthorhombic $P2_12_12_1$ or $Pca2_1$ could again relieve the instabilities, but this time fifty four crystallographic M sites would be created. A more plausible transition would seem to be to orthorhombic $P2_12_12_1$ or $Pca2_1$ but without the 3 x 3 x 3 superstructure. However, such a transition apparently does not occur for this structure type.

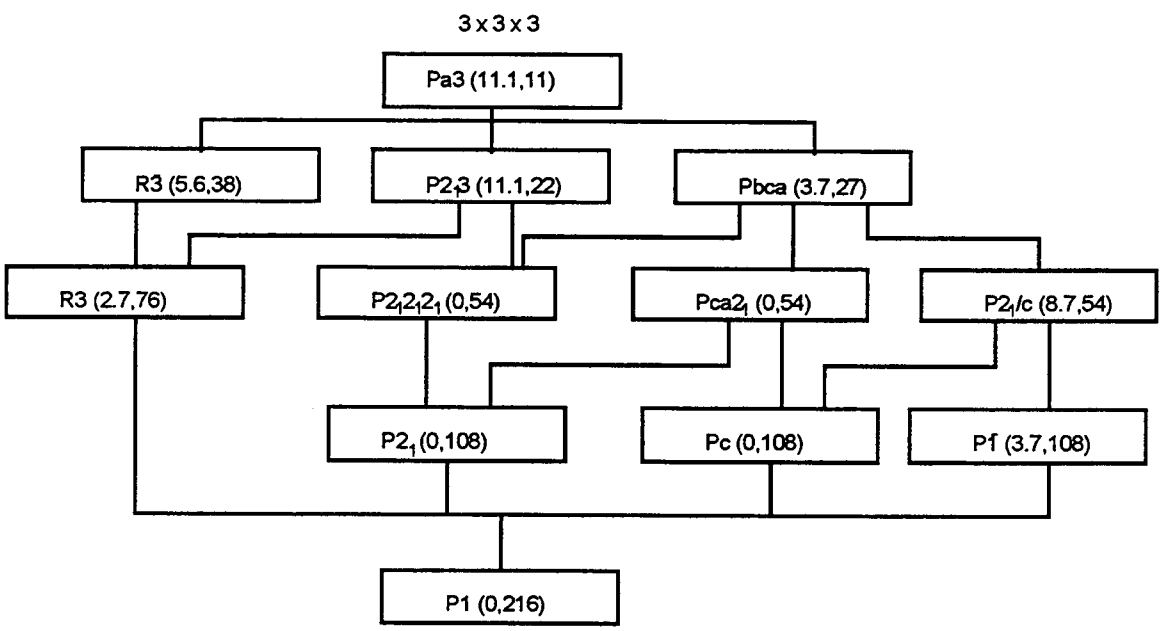

Figure 6.11 Possible Space Groups for Tripled unit cell of $A^{4+}M^{5+}{}_2O_7$

6.5 References

1. Giorgio Peyronel, *Gazz. Chim. Ital.*, **72**, 77-83 (1942)

2. Y. Tsujii, E. Miura, M. Hashiba, Y. Nurishi, and T. Hibino, *Gifu Diagaku Kogakubu Kenkyu Hokoku*, **28**, 89 (1978)

3. J. Alamo, and R. Roy, *J. Am. Ceram. Soc.*, **67**, 78-80 (1984).

4. G. Lenain, H.A. McKinstry, S.Y. Limaye, and Woodard, *Mat. Res. Bull.*, **19**, 1451-1456 (1984)

5. R. Roy, D.K. Agrawal, J. Alamo and R.A. Roy, *Mat. Res. Bull.*, **19**, 471-477, (1984)

6. Sridhar Komarneni, *Int. J. High Tech. Cer.*, **4**, 31-39 (1988)

7. Toshitaka Oota and Iwao Yamai, *J. Am. Ceram. Soc.*, **69**, 1-6 (1986)

8. D.E. Harrison, H.A. McKinattry, and F.A. Hummel, *J. Am. Ceram. Soc.*, **37:6**, 277-280 (1954)

9. .H. Gillery and E.A. Bush, *J. Am. Ceram. Soc.*, **42**, 174-177 (1979)

10. D. Taylor, *Br. Ceram. Trans. J.*, **83**, 5-9 (1984)

11. KR. Laud and R.A. Hummel, *J. Am. Ceram. Soc.*, **54**, 296-298 (1971)

12. D.E. Harrison, and R.A. Hummel, *J. Am. Ceram. Soc.*, **42**, 487 (1959)

13. K.M. Merz, H.T. Smyth, H.P. Kirchner and J.L. Beal, Cornell Aeronautical Lab., Report No. PI-1273-M-8 (1960)

14. D.E. Harrison, H.A. McKinstry and F.A. Hummel, *J. Am. Ceram. Soc.*, **37**, 277-280 (1954)

15. A. Burdese and M. Lucco Borlera, *Ann. Chim. Rome*, **53**, 333-343 (1969)

16. A. Burdese and M. Lucco Borlera, *Atti. Acad. Sci. Torinao. Cl. Sci. Fis. Mater. Nat.*, **94**, 107-120 (1959)

17. C.H. Huang, O. Knop and D.A. Othen, *Can. J. Chem.*, **53**, 79-91 (1975)

18. H. Vollenkle, A.Wittman and H. Nowotny, *Monatsh. Chem.*, **94**, 956 (1963)

19. L.O. Hagman and P. Kierkegaard, *Acta Chem. Scand.*, **23**, 327 (1969)

20. B. Wellmann, Liebau, *J. Less Common Metals*, **77(2)**, 31 (1981)

21. F. Liebau, G. Bissert and N. Koppen, *Z. Anorg. Allg. Chem.*, **359(3-4)** p. 113 (1968)

22. L.O. Hagman and P. Kierkeguard, *Acta Chem. Scand.*, **23**, 327 (1969)

23. N. Kinomura, M. Hirose, N. Kumada nad F. Muto, *Mat. Res. Bull.*, **20**, 379 (1985)

24. C.W. Bjorklund, *J. Am. Chem. Soc.*, **79**, 6347 (1957)

25. S. Oyetola, A. Verbaere, D. Guyomard, M.P. Crosnier, Y Piffard and M. Tournoux, *Eur. J. Solid State Inorg. Chem.*, **28**, 23-36 (1991)

26. A. Verbaera, S. Oyelola, D. Guyomard and Y. Piffard, *J. Solid State Chem.*, **75**, 217-224 (1988)

27. S. Z. Haider, *Anal. Chimica Acta*, **24**, 250 (1961)

28. O. Hajo, *Naturwissenschaften.*, **52**, 344 (1965)

29. G. LeFlem. J. Lamic and P. Hagenmuller, *Memaires Presentes A La Societe Chimique*, 1880-1883 (June 1966)

30. D. F. Craig and F.A. Hummel, *J. Am. Ceram. Soc.*, **55**, 532 (1972)

31. R.C. Buchanan and G.W. Wolter, *J. Electrochem. Soc.*, **130:9**, 1965-1910 (1983)

32. N. Roberts, W. W. Warren and R. Dupree, Private Communication, Department of physics, Oregon State University

33. W.M. Meir and H. Villiger, *Z. Kristallogr.*, **129**, 161-185 (1966)

34. R. Hubin and P. Tarte, *Spectrochemica Acta*, 23A, 18-15-1829 (1967)

35. Von I.L. Botto and E.J. Baran, *Z. Anorg. Allg. Chem.*, **430**, 283-288 (1977)

36. Guido Busca et. al., *J. of Catalysis,* **99**, 400-414 (1986)

37. A.I. Teterevkov and V.I. Poloiko, *Russian J. of Inorg. Chem.*, **27(4)**, 604-605 (1982)

BIBLIOGRAPHY

Alamo, J. and Roy, R., *J. Am. Ceram. Soc.*, **67**, 78-80 (1984)

Armstrong, R.D., Dickinson, T. and Willis, P.M., *Electroanal. Chem. and Interfacial Electrochem.*, **53**, 389-405, (1974)

Aurivillius, B., Lindblom, C.-I., and Stenson, P., *Acta Chem. Scand.*, **18(6)**, 1555 (1964)

Bachmann, H.G., Ahmed, F.R., and Barnes, W.Z., *Z. Kristallogr.*, **115**, 110 (1961)

Bement ,A.L., et. al.,"Materials and Processing Report", **4[3]**, June 1989

Bergman, A.G., and Sanzharova, Z.I., *Russ. J. of Inorg. Chem.*, **15**(4), 581-582 (1970)

Bergman, A.G., and Sanzharova, Z.I., *Russ.J. of Inorg. Chemistry*, **15**(6), 877-878 (1970)

Bhargava, R.N. and Condrate, A. SR., *Applied Spectroscopy*, **31**(3),230-236 (1977)

Bjorklund, C.W., *J. Am. Chem. Soc.*, **79**, 6347 (1957)

Bordes, E. and Courtine, P., *Journal of Catalysis*, **57**, 236-252 (1979)

Botto, Von I.L. and Baran, E.J., *Z. Anorg. Allg. Chem.*, **430**, 283-288 (1977)

Brown, J.J. and Hummel, F.A., *Trans. Brit. Ceramic Soc.*, **64**, 419 (1965)

Bruton, E., "Diamonds", N.A.G. Press LTD., London, 300-307 (1970)

Buchanan, R.C. and Wolter, G.W., *J. Electrochem. Soc.*, **130:9**, 1965-1910 (1983)

Burdese, A. and LuccoBorlera, M., Ann. Chim. Rome, **53**, 333-343 (1969)

Burdese, A. and LuccoBorlera, M., *Atti. Acad. Sci. Torinao. Cl. Sci. Fis. Mater. Nat.*, **94**, 107-120 (1959)

Busca, Guido et. al., *J. of Catalysis*, **99**, 400-414 (1986)

Bush, A. A., Koshelayeva, V.G. and Venentsev, Yu.N., *Jap. J. Appl. Phys.*, **24(2)**, 625 (1985)

Casal, B., Ruiz-Hitzky, E., Crespin, M., Tinet, D., Galvan, J.C., *J. Chem. Soc., Faraday Trans.*, **85**, 4167, (1989)

Caton, Gloria M. et. al., "Ceramic Technology Newsletter", Ceramic technology project, Oak ridge national labs and Department of Energy under contract DE-AC05-84OR21400, January-March, No 42

Craig, D.F. and Hummel, F.A., *J. Am. Ceram. Soc.*, **55**, 532 (1972)

Cromer, D.T. Liberman, D., *J. Chem. Phys.*, **53**, 1891, (1970).

Cromer, D.T., Mann, J.B., *Acta Crystallogr.*, Sect. A , **24**, 321, (1968).

Crystallographic Computing 3, Eds. Sheldrick, G.M., Kruger, C., and Goddard, R., Oxford University Press, 1985, pp. 175-189.

Crystallographic Computing 3; Eds. Sheldrick, G.M., Kruger, C., and Goddard, R., Oxford University Press, 1985, pp. 175-189.

Dumbaugh, W.H., Jr., and Malmendier, J.W., "Refractory Glasses", *High Temperature Oxides, Part IV*, Academic Press, New York and London, 1-14 (1971)

Horr, N.El, Hammou, A., Bagieu, M., *J. Solid State Chem.*, **90**, 361-366 (1991)

Gillery, F.H. and Bush, E.A., *J. Am. Ceram. Soc.*, **42**[4], 174-177 (1979)

Gopal, R. and Calvo, C., *J. Solid State Chem.*, **5**, 432 (1972)

Hagman, L.O. and Kierkegaard, P., *Acta Chem. Scand.*, **23**, 327 (1969)

Hagman, L.O. and Kierkeguard, P., *Acta Chem. Scand.*, **23**, 327 (1969)

Haider, S.Z., *Anal. Chimica Acta*, **24** 250 (1961)

Hajo O., *Naturwissenschaften.*, **52**, 344 (1965)

Hardcastle, R.D., Ph.D. Thesis, Lehigh University (1990)

Harrison, D.E. and Hummel, R.A., *J. Am. Ceram. Soc.*, **42**, 487 (1959)

Harrison, D.E., McKinattry, H.A. and Hummel, F.A., *J. Am. Ceram. Soc.*, **37:6**, 277-280 (1954)

Hodge, I.M., Ingram, M.D. and West, A.R., *Electroanal. Chem. an Interfacial Electrochem.*, **58**, 429-432, (1975)

Hodge, I.M., Ingram, M.D. and West, A.R., *J. Electroanal. Chem.*, **74**, 125-143 (1976)

Holcombe, C.E., Jr., *Am. Ceram. Soc. Bull.*, **59[12]**, 1219 (1980)

Huang, C.H., Knop, O. and Othen, D.A., *Can. J. Chem.*, **53**, 79-91 (1975)

Hubin, R. and Tarte, P., *Spectrochemica Acta*, 23A, 18-15-1829 (1967)

Hummel, F.A., *Interceram*, **33[6]**, 27-30 (1984)

Illarionov, V.V., Soklakov, A.I. and Kil'disheva, E.V., *Russ. J. of Inorg. Chem*, **6**(6), 696-699, (1961)

Illarionov, V.V., Ozerov, R.P. and Kil'disheva, E.V., *Russ. J. Inorg. Chem.*, **5**(12), 1352 (1960).

Jordan, B. and Calvo, C., *Canad. J. Chem.*, **51**, 2621 (1973)

Kinomura, N., Hirose, M., Kumada, N. and Muto, F., *Mat. Res. Bull.*, **20**, 379 (1985)

Kirchner, H.P., Merz, K.M. and Brown, W.R., *J. Am. Ceram. Soc.*, **46[3]**, 137 (1963)

Komarneni, Sridhar, *Int. J. High Tech. Cer.*, **4**, 31-39 (1988)

Korthuis, V.C., Hoffmann, R.D., Huang, Jinfan and Sleight, A.W., Chemistry of Materials, **5(2)**, 206, 1993

Korthuis, V., Hoffmann, R.D., Huang, Jinfan and Sleight, A.W., *J. Solid State Chem.*, **105**, 294-299 (1993)

Korthuis, V.C., Hoffmann, R.D., Huang, Jinfan, and Sleight, A.W., *J. Solid State Chemistry*, **105**, 294, (1993)

Land, K.R. and Hummel, F.A., *J. Am. Ceram. Soc.*, **54[8]**, 407 (1971)

Landsberg, F.R. and Bray, P.J., *J. Chem. Phys.*, **53**, 2757 (1970)

Laud, KR. and Hummel, R.A., *J. Am. Ceram. Soc.*, **54**, 296-298 (1971)

LeFlem, G., Lamic, J. and Hagenmuller, P., *Memaires Presentes A La Societe Chimique*, 1880-1883 (?)

Lenain, G.E., Mckinstry, H.A., Limaye, S.Y., and Woodward, A., *Mat. Res. Bull.*, **19[11]**, 1451 (1984)

Lenain, G., McKinstry, H.A., Limaye, S.Y. and Woodard, *Mat. Res. Bull.*, **19**, 1451-1456 (1984)

Liebau, F., Bissert, G. and Koppen, N., *Z. Anorg. Allg. Chem.*, **359**(3-4) p. 113 (1968)

Manning, W.R., Hunter, O.,Jr., Calderwood, F.W. and Stacy, D.W., *J. Am. Ceram. Soc.*, **55[7]**, 342 (1972).

Meier, W.M. and Villiger, H., *Z. Kristallogr.*, **129**, 161-185 (1966)

Merz, K.M., Smyth, H.T., Kirchner, H.P. and Beal, J.L., Cornell Aeronautical Lab., Report No. PI-1273-M-8 (1960)

Miolberg, M.E., and Blair, H.D., *J. Am. Ceram. Soc.*, **60[7-8]**, 372 (1977)

Moya, J.S., Verduch, A.G. and Hortal, M., *Trans. & Journ. of British Ceram. Soc.*, **73[6]**, 177 (1974)

Oliveira, A.L., Damasceno, O.O., Oliveira, J. and Schouler, E.J.L., *Mater. Res. Bull.*, **21**, 877 (1986)

Oota, Toshitaka and Yamai, Iwao, J. Am. Ceram. Soc., **69**[1], 1-6 (1986)

Ostertag, W., Fischer, G.R. and Williams, J.P., *J. Am. Ceram. Soc.*, **51[11]**,651 (1968)

Oyetola, S., Verbaere, A., Guyomard, D., Crosnier, M.P., Piffard, Y. and Tournoux, M., *Eur. J. Solid State Inorg. Chem.*, 28, 23-36 (1991)

Peyronel, G., *Gazz. Chim. Ital.*, **72**, 77 (1942)

Peyronel, Giorgio, *Gazz. Chim. Ital.*, **72**, 77-83 (1942)

Powder Diffraction File, JCPDS International Centre for Diffraction Data, Swarthmore, PA

Preuss, Fritz and Schug, Heinrich, *Z. Naturforsh. 30 b*, 334-339 (1975)

Roberts, N., Warren, W.W. and Dupree, R., Private Communication, Department of physics, Oregon State University

Roy, R., Agrawal, D.K., Alamo, J. and Roy, R.A., *Mat. Res. Bull.*, **19**, 471-477, (1984)

Struck, C.W. and White, J.G., *Acta Cryst.*, **15**, 290 (1962)

Toshihiko, T., Kozaburo, Y., Yukiko, Kobayashi, I.Y. and Shiegeo, H., (Sharp Corporation) **Jpn. Kokai Yokkyo Koho JP 63 61,079; 63 61,080;** September 2, 1986

Taylor, D., *Br. Ceram. Trans. J.*,**83**, 5-9 (1984)

Teterevkov, A.I. and Poloiko, V.I., *Russian J. of Inorg. Chem.*, **27(4)**, 604-605 (1982)

TEXSAN, Molecular Structure Corporation, The Woodlands, TX , USA (1988).

Tsujii, Y., Miura, E., Hashiba, M., Nurishi, Y. and Hibino, T., *Gifu Diagaku Kogakubu Kenkyu Hokoku*, **28**, 89 (1978)

Verbaera, A., Oyelola, S., Guyomard, D. and Piffard, Y., *J. Solid State Chem.*, **75**, 217-224 (1988)

Vollenkle, H., Wittman, A. and Nowotny, H., *Monatsh. Chem.*, **94**, 956 (1963)

Wellmann, B., Liebau, *J. Less Common Metals*, **77(2)**, 31 (1981)

West, A.R., *Solid State Chemistry and its applications*, John Wiley and Sons (1984), Chapt. 13

West, A.R., *Solid State Chemistry and its applications*, John Wiley and Sons (1984), Appendix A8

Yvon, K., Jeitschko, W. and Parthe, E., *J. Appl. Cryst.* **10**, 73 (1977).

Zhou, Wuzong, *J. Solid State Chem.*, **76**, 290 (1988)

APPENDIX

Appendix A Operation of the Netzsh Dilatometer

A.1 Introduction to Thermal Mechanical analysis

The dilatometer is used to measure the mechanical response of a material as a function of temperature. This has been termed thermal mechanical analysis (TMA). The basic setup of a dilatometer apparatus is shown in Figure A.1. The pushrod and sample support are made out of the

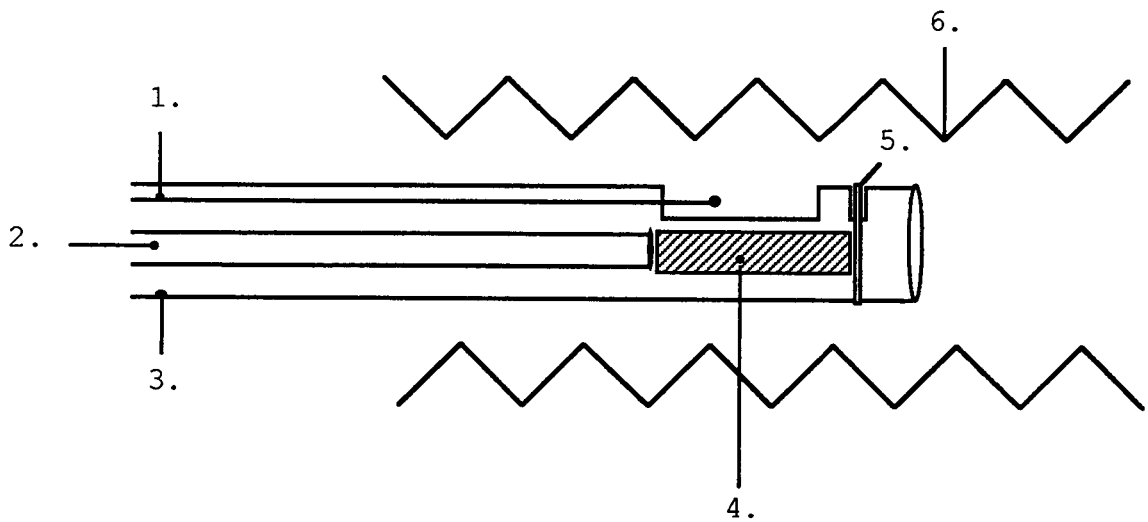

Figure A.1 Major features of the dilatometer; (1) type S thermocouple, (2) pushrod, (3) sample support, (4) sample, (5) sample stopper, (6) heater coils.

material which is either alumina for high temperature measurements or quartz for lower temperature measurements. The coefficient of linear expansion, which is defined in Table A.1, for silica is much smaller (α = 0.5 x 10^{-6}) than alumina and thus has an increased accuracy.

Table A.1

Definitions for Thermal Mechanical Analysis

Coefficient of Linear Expansion	$\alpha = \frac{\Delta L}{L_i \Delta T}$	($\mu m/(\mu m°C)$)
Relative Expansion	$\frac{\Delta L}{L_i}$	
	$\Delta L = L_f - L_i$	(μm)
	$\Delta T = T_f - T_i$	(°C)

In order to obtain good data one must correct the dilatometer by running a sample with a known thermal expansion coefficient. We have two crystals of sapphire (Al_2O_3), with two different lengths (25.86 and 21.72 mm). The theoretical curve for the sapphire is stored in the software and the difference between the theoretical and

experimental data is fitted to a tenth degree polynomial which is called the correction curve for the dilatometer. This correction curve is then added to subsequent data.

One must however be aware that the samples one prepares are going to be of different lengths than the standards. This is corrected for in the software in the following way. If one uses the 25.86 mm sapphire standard which has an $\alpha \sim 7.8 \times 10^{-6}$ from 20 °C to 800°C, the standard should have expanded by 157.3 μm (i.e. 7.8×10^{-6} $°C^{-1}$ x (800-20 °C) x 25.86 mm). But one must remember that the sample support and pushrod expand also, and one may expand faster than the other thus leading to the correction curve. One should notice that the support should contract and expand independently of sample size. The amount of pushrod in the hot zone is the only difference between any type of sample size. To be able to correct for sample size differences one must correct for different amounts of pushrod in the hot zone. The software accomplishes this by taking the correction curve and multiplying by the ratio of standard and new sample length.

For example, if the sample was 23 mm and the standard was 25.86 mm then one would multiply 23/25.86 of the correction value at that temperature. Notice that in the above example there is more pushrod in the hot zone and

thus the correction should be less since the pushrod and sample support are made of the same material.

A.2 Operation of Dilatometer

First one must calibrate the instrument. First place the standard in the sample support, noting the length of the standard. Place all color coded cables in the corresponding plugs. Place the range selector switch on the carrier frequency measuring amplifier shown in Figure A.2 to 500 μm. Dial the length correction and R-balance to zero. Turn the dial on the dilatometer to move the pushrod against the standard. Continue turning until the tuning indicator is deviated all the way to the left and the output voltage amplifier is in the center. Switch the range to lower values and continue turning the dial on the dilatometer until the output voltage indicator is in the middle.

Run the calibration run routine in the software. One must note that you cannot do a calibration run ramping up and then down in temperature. This is because the program will try to fit a difference curve as explained above to a curve which will have two different points at the same

temperature. Program the furnace to go up to 850 °C at 5°C/min and then end. Turn the range selector switch to the desired range noting that if you choose for example 500 µm the range will be +250 to -250 microns.

In the software portion there is a bug. When one comes to the INPUT DATA DISPLAY menu the EXP RANGE microns FS (Q) is the value on the range selector switch but one

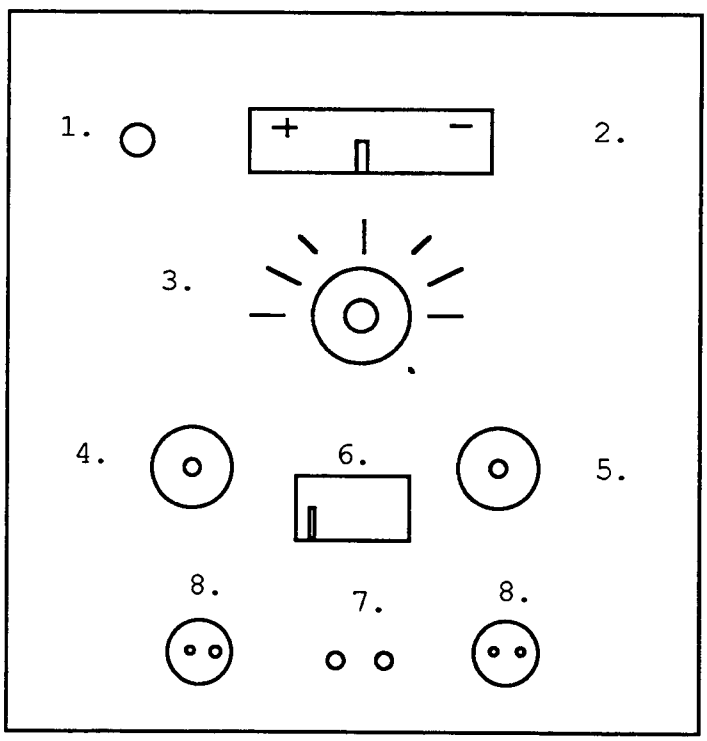

Figure A.2 Carrier frequency measuring amplifier. (1) Calibration button, (2) Output voltage amplifier, (3) Range selector switch, (4) Length correction, (5) R-balance, (6) Tuning Indicator for bridge balance, (7) Power switch, (8) Cable input plugs

must divide this value by 10. Therefore if the range selector switch is on 500 μm the value here should be 50. Proceed as normal to start the run. When it has finished answer yes to the apply dilatometer correction. One should periodically do this say every 3 months, depending on how many runs have been carried out, and especially if the dilatometer is moved or the pushrod and sample support have been changed.

The same procedure is used for running your samples except one chooses sample run instead of calibration run. One can ramp up and down with a sample but one must note that the run down will not be truly corrected for. The furnace is not able to ramp down with the same accuracy as it can ramp up in temperature. To be able to see the data come back down to room temperature one can tell the computer you want to hold (feature N.), and give a time in the isothermal time (feature O.) of say 80 minutes. This is because the computer calculates how much time it will take based on ramp rates to ramp up and down, then divides this by the maximum number of data points to take readings at this interval. The furnace itself once it is ramping down cannot keep pace with the program and the cooling rate will be much slower than the programmed heating rate. Therefore all calculations on your data should be done on the increasing temperature curve.

The software also has a feature to convert the binary data to ascii, to be imported into spreadsheet programs. This does not work. I have written two programs called BIN2ASC and ASC2BIN that are available on the computer. The output consists of comma delimited values of time, temperature and raw expansion (μm). Even though the program has a feature to store data it will not store corrected data. Tuning of the amplifier itself should be done periodically. The amplifier was very much out of tune when it was received and has been tuned and no significant drift was observed. The amplifier tuning is described in the material that came with the instrument.